Politecnico di Torino

Dipartimento di Scienza Applicata e Tecnologia (DISAT)

Biomedical Engineering

Master Thesis

In-vitro Evaluation of Bioactivity, Biodegradation and Molecule Uptake/Release Properties of Porous ZnO Structures for Tissue Engineering

Sonia Atienza Albiac

Academic Supervisor: Dr. Marco Laurenti

Tutor: Prof. Valentina Cauda

Academic Year 2016-2017

ACKNOWLEDGEMENTS

I wish to express my most sincere gratitude to my academic supervisor, Dr. Marco Laurenti, for his guidance, patience, suggestions and advice throughout the development of the thesis. Besides, I have also acquired valuable insights through his instructions.

I would also like to wish my deepest thanks to Prof. Valentina Cauda for giving me the opportunity of doing the thesis at the TNH Research Lab. Also for guiding, instructing and assisting me during the development of my program of study at Politecnico di Torino. Without whose help the thesis wouldn't have been successful.

I would also like to thank all the members from the TNH Research Lab for helping me anytime I need them.

Last but not least, thanks to Prof. Chiara Vitale Brovarone, and specially to Dr. Giulia Molino for letting me do part of my experimental activity in their laboratory: BOOST Research Lab.

CONTENTS

Chapter 1. Introduction and objectives

This work focuses on the investigation of the bioactivity, biodegradation behaviour and uptake/release properties of porous zinc oxide (ZnO) thin films deposited by sputtering technique. The final aim consists of coupling all these properties into a single platform, that would result into novel ZnO-based biomaterials for tissue engineering and drug delivery applications.

In the first part of the work, the interactions of the porous ZnO structures with Simulated Body Fluid (SBF) and the medium for cell culture (eMEM) have been investigated for studying their bioactivity and biodegradation. In the case of the bioactivity study, the porous ZnO samples have been also coated with graphene oxide (GO) flakes, in order to investigate the influence of GO on the bioactivity of porous ZnO.

As a second part, this thesis work is also focused on the investigation of porous ZnO films for drug delivery applications. Rhodamine-B has been used as a fluorescent molecule for studying the capacity of porous ZnO thin films to uptake and further release molecules, for future drug delivery applications.

The experimental activity has been focused on the implementation of the experiments for evaluating the bioactive and biodegradation properties of the ZnO samples when interacting with the media mentioned above (SBF and eMEM). Each sample has been properly investigated in terms of morphology, crystal structure and chemical composition. The activities have been developed at the Dipartimento di Scienza Applicata e Tecnologia (DISAT) of Politecnico di Torino, specifically at the TNH Research Lab of Professor Valentina Cauda and BOOST Research Lab of Professor Chiara Vitale Brovarone.

The basic scheme of this thesis can be summarized as follows. Chapter 2 provides a brief background theory introduction, especially focused on a general description of the bioactivity, biocompatibility and antibacterial properties of ZnO and GO, hydroxyapatite (HAp) precipitation phenomena, and finally SBF solution and eMEM. This is followed by Chapter 3, reporting a description of the materials and methods followed to prepare and characterize all the investigated samples, as well as to study the bioactivity, biodegradation and uptake/release abilities. It is also reported a description of the physicochemical principles and the characterization setups that have been used in this thesis. All the experimental results are summarized in Chapter 4. Chapter 5 reports the main conclusions of the thesis work.

Chapter 2. Background theory

The aim of this chapter is to introduce and describe the materials used in this thesis work. The attention will be focused on their bioactivity, biodegradability and biocompatibility.

2.1 Tissue engineering

Tissue engineering (TE) is a process belonging to regenerative medicine, consisting of the combination of several strategies to improve and/or repair biological tissues. TE strategies involve three major elements: cells, signalling molecules, and natural or artificial scaffolds. A scaffold is a structure of artificial or natural materials on which tissue is grown to mimic a biological process outside the body or to replace a disease or damaged tissue inside the body. Scaffolds for use in regenerative medicine provide the base for the repopulation and specialization of stem cells, blood vessels and extracellular matrices. In general, the surface morphology of the scaffold strongly affects the attachment of surrounding cells and tissues after implantation. Recently [1], nanomaterials have been investigated for use as biomaterials. Nanostructures at the surface of the underlying material enhance some bioactivities due to quantum size effects and their large surface area. Thanks to the combination of these properties the contact between regenerative cells or tissues and the nanostructures can be beneficial for promoting cell physiological proliferation or regeneration.

For example, previous studies [2] reported that ZnO containing nano-hydroxyapatite/chitosan cement is a promising material to enhance bone regeneration in osseous defect sites. Therefore, our hypothesis was that soaking ZnO samples into SBF solution and medium for cell culture would provide precipitation of hydroxyapatite (HAp) to the scaffold. Also, by modifying the sample using GO coating, there was expected to obtain a further enhancement of bioactive and drug delivery properties.

2.2 Zinc oxide

Zinc Oxide is a semiconductor of the II-IV group [3] showing several favourable properties. It has a wide band gap energy of 3.37 eV, a strong room-temperature luminescence, absorption of light in the UV range, a high electron mobility and high thermal conductivity [4, 5]. Moreover, it shows biocompatibility and low impact on the environment when being disposed at the end of its life cycle [6].
Among semiconductors, ZnO is one of the most investigated thanks to the possibility of combining its semiconducting behaviour with its promising catalytic, electrical, optical and piezoelectric properties [6]. Furthermore, it can be easily synthesized in a large amount of shapes and sizes. Also, it can be deposited using various methods including: physical or chemical vapour deposition (PVD or CVD), pulsed laser deposition, radio frequency (RF) magnetron sputtering, etc.

ZnO has a wurtzite crystal structure at ambient conditions, showing a hexagonal unit cell with two lattice parameters, a and c. *Figure 1* clearly shows that the structure is composed of two interpenetrating hexagonal closed packed (hcp) sublattices, in which each consist of one type of atom (Zn or O) displaced with respect to each other along the threefold c-axis. It can be simply explained schematically as a number of alternating planes stacked layer-by-layer along the c-axis direction and composed of tetrahedrally coordinated Zn^{2+} and O^{2-}. The tetrahedral coordination of ZnO gives rise to the non-centrosymmetric structure. In wurtzite hexagonal ZnO, each anion is surrounded by four cations at the corners of the tetrahedron, which shows the tetrahedral coordination and hence exhibits the sp3 covalent-bonding. The two important characteristics of the wurtzite structure are the noncentral symmetry and polar surfaces.

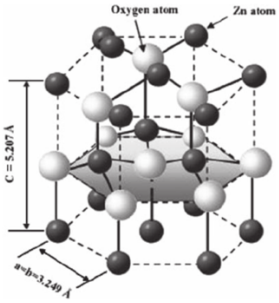

Figure 1: The hexagonal wurtzite structure model of ZnO. The tetrahedral coordination of Zn-O is shown. O atoms are shown as larger white spheres while the Zn atoms are smaller brown spheres

Reflecting the basic properties of ZnO, oxide nanoparticles have antibacterial properties and for this reason they are added to materials such as cotton, rubber, oral care products, and food packaging [7]. We mentioned ZnO nanoparticles because some studies demonstrate that these particles exhibit both qualitatively and quantitatively better antibacterial properties than bulk ZnO with a particle size of 2 μm. So, ZnO exhibit strong activity even when administered in small amounts. The activity is quantitatively evaluated by studying the growth medium caused by the bacterial metabolism. As ZnO is an antibacterial material, when administered, there is shown a bacterial growth inhibition. As smaller is the ZnO nanoparticle the most growth inhibition is obtained. The considerable antibacterial activity ZnO is attributed to the generation of reactive oxygen species on the surface of this oxide, studied by a conductometry, which is method that monitors the capability of the analyte to conduct an electrical current [8].

The advantage of using this metal oxide as antimicrobial agent is that it contains the following mineral elements essential to humans: calcium, phosphorous, magnesium, zinc, chlorine and others. Those elements are called essential to humans because without them our body won't function properly. For example: calcium is needed for the construction and maintenance of bone and normal function of nerves and muscles and phosphorous is an important constituent of adenosine triphosphate.

Inorganic nanocrystalline metal oxides are particularly interesting because they can be prepared with extremely high surface areas, and are more suitable for biological applications. The advantages of inorganic antibacterial materials over organic antibacterial materials are that the former show superior durability, less toxicity and greater selectivity and heat resistance. ZnO has been extensively studied as antimicrobial agent due to its photocatalytic activity under UV light [9] [10]. ZnO can highly absorb UV light and it has a better response to UV light, thus its conductivity dramatically enhances, and this feature significantly activates the interaction of ZnO with bacteria.

Bioactivity of ZnO nanomaterials have been demonstrated by studying the antimicrobial activity of suspensions with various particle sizes. The bioactivity of smaller particles is attributed to the higher surface area to volume ratio. For smaller ZnO nanoparticles, more particles are needed to cover a bacterial colony (2 μm) which results in the generation of a larger number of active oxygen species, which kill bacteria more effectively

One of the most important features of ZnO nanomaterials is biodegradability. Zn^{2+} is an indispensable trace element for adults and it is involved in various aspects of metabolism. Chemically, the surface of ZnO is rich in ^{-}OH groups, which can be readily functionalized by various surface decorating molecules [11, 12]. ZnO can slowly dissolve in both acidic (e.g. in the tumour cells and tumour microenvironment) and strong basic conditions if the surface is in direct contact with the solution [13].

Also, ZnO nanomaterials are versatile nanoplatforms for drug delivery applications, due to their large surface area, versatile surface chemistry, phototoxic effect, among others. In vitro studies have shown that ZnO nanoparticles can be highly toxic to cancer cells [14] or bacteria and leukemic T cells [15]. Therefore, ZnO nanomaterials have been investigated as drug/gene delivery vehicles, and also studied for cancer therapy.

For applications of nanomaterials in biomedicine, the biocompatibility is always a concern. Even though ZnO has been approved for cosmetic uses, the detailed toxicological profile and the mechanism of cytotoxicity for ZnO nanomaterials is not clear. Many studies have focused on the biocompatibility of ZnO nanomaterials without surface coating/modifications. For example, it was reported that ZnO nanoparticles showed cytotoxic effect above certain concentrations and the toxicity was pH dependent, due to the increased concentration of Zn^{2+} in the culture medium or inside cells from dissolved ZnO [16]. Nonetheless, such leakage of ionic Zn^{2+} into the biological system from dissolution of ZnO can perhaps be well-tolerated since ~10 mg/day of Zn^{2+} is needed for adults. Meanwhile, other reports have shown that ZnO nanomaterials were nontoxic and preferentially toxic to bacteria or cancer cells [15, 14] which could be advantageous for both antibacterial and cancer therapy applications.

Surface modification of nanomaterials plays a crucial role for potential biomedical applications. It has been demonstrated that the biocompatibility of ZnO nanomaterials could be improved by slowing down the dissolution rate through Fe doping [17] or surface capping [18].

There are different types of ZnO nanostructures as nanoparticles, nanorings, nanowires, depending on the desirable application.

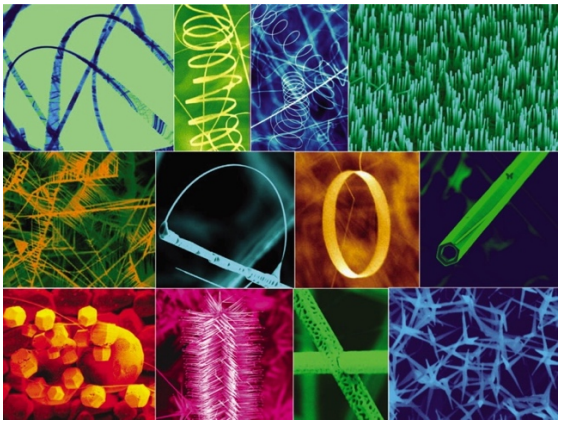

Figure 2: A collection of nanostructures of ZnO synthesized under controlled conditions by thermal evaporation of solid powders. Most of the structures presented can be produced with 100% purity [19].

Nanoparticles are essentially a varied form of basic elements derived by altering their atomic and molecular properties of elements. ZnO nanoparticles exhibit antibacterial, anti-corrosive, antifungal and UV filtering properties [20].

In a recent study [21], ZnO nanoparticles were synthesized using various routes. The sol–gel method proved a successful synthetic route in terms of its cost, ease of handling, reliability, repeatability, and environmental friendliness. Moreover, with detailed review, it is confirmed that the various applications of ZnO nanoparticles depend upon the control of both physical and chemical properties such as size, size distribution, shape, surface state, crystal structure and organization onto a support. In addition, these factors mainly depend upon the synthetic method. Therefore, shape, size and dispersity can be controlled by tuning different parameters during the synthesis process, e.g., the precursor type and concentration, types of capping molecule, types of solvent, reaction time, and reaction temperature. Application of ZnO nanoparticles in the biological realm requires high quality ZnO nanoparticles in aqueous solution at neutral pH and physiological temperature, because biomolecules are very sensitive to changes in temperature and pH. In addition, relatively small size, ease of transport within tissues/organs, ability to cross plasma membranes, and potential targeting of biologically active molecules will facilitate biomedical applications of nanoparticles in the field of medicine.

ZnO nanowires have a typical length that can vary from 100 μm to 1 mm and the diameter is in the range of 50-500 nm. The porous structure of the ZnO nanowires is apparent. The high-porosity, single-crystal wire-like structures have potential applications as filters, catalyst supports, and gas sensors.

Highly oriented and transparent ZnO thin films have significally been researched because of their potential application in transparent electrode in displays, window layers in solar cells, field emitters, ultraviolet laser emission, photodetectors, bio-sensors, etc.

ZnO thin films can be prepared by techniques such as thermal oxidation, chemical vapour deposition, molecular beam epitaxy and pulsed laser deposition. The technique of Radio Frequency (RF) sputtering has drawn considerable attention for ZnO film fabrication since the resulting film properties can be controlled by changing the sputtering conditions such as substrate temperature, deposition time, pressure, and RF power.

In this thesis porous ZnO thin films have been the material of the samples used. Made by a huge amount of ZnO nanoparticles interconnected to each others, this is the reason why they are considered nano objects as well.

2.3 Graphene oxide as a coating

Graphene is a carbon based material that can be viewed as a one atom thick sheet of graphite. Because high quality sheets of graphene are often prepared by chemical vapour deposition (CVD) [22] [23], which requires expensive equipment, many groups have looked at using graphene oxide (GO) as a solution processable alternative for the preparation of graphene-like materials [24] [25] [26]. Indeed, graphene oxide can be reduced in solution and as a thin film using a variety of reducing conditions, and reduction converts the graphene oxide into a material that has a large enhancement in electrical conductivity [26] [27]. In addition to its use in making reduced graphene oxide for electronic devices, graphene oxide has been used in catalytic oxidation, energy storage, cell imaging and drug delivery applications, as well as biosensors.

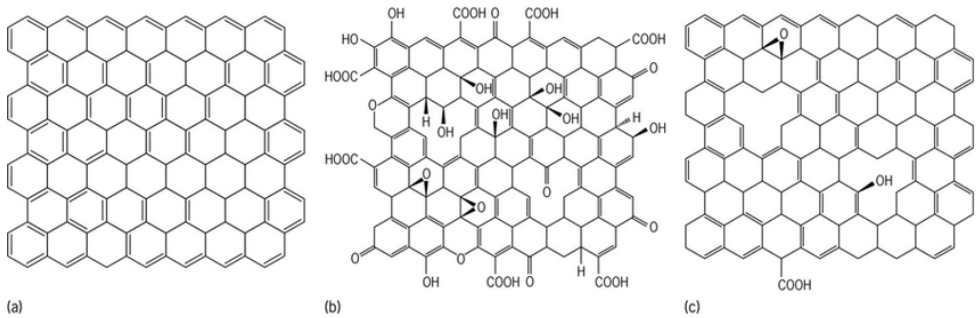

Figure 3: Chemical structure of graphene (a), graphene oxide (b) and reduced graphene oxide (c)

Since, in 2008, the use of graphene oxide (GO) as an efficient nanocarrier for drug delivery was reported [28] a lot of interesting work has been carried out to explore the use of graphene for widespread biomedical applications, ranging from drug/gene delivery, biological sensing and imaging, antibacterial materials, to biocompatible scaffold for cell culture. The intensive research on the bioapplications of graphene and its derivatives is due to many fascinating properties, such as high specific surface area (2630 m^2/g), exceptional electronic conductivity (mobility of charge carriers, 200,000 $cm^2 V^{-1} s^{-1}$), thermal conductivity (~5000 W/m/K), mechanical strength (Young's modulus, ~1100 Gpa) of graphene, and, intrinsic biocompatibility, low cost and scalable production, and facile biological/chemical functionalization of GO [29, 30].

For using GO in biomedical applications it's essential to know its toxicity. Recent studies have demonstrated some cellular cytotoxicity of graphene that may cause less cellular adhesion and induce cellular apoptosis. Nevertheless, by introducing functional groups on graphene surface, the interaction between GO and tissue or cells and the generation of reactive species of oxygen is reduced, due to the presence of carboxylic, epoxy and hydroxide groups. So, it is necessary to functionalized GO layers in order to use it in biomedical applications [31].

As it is mentioned above, GO can promote biological interactions due to its many surface functional groups (e.g. hydroxyl, epoxide, and carbonyl). Several investigators have reported that GO can serve as a carrier for drugs and other biomolecules. In addition, GO regulates the proliferation and differentiation of cultured mesenchymal stem cells and improves the properties of scaffolds. Subcutaneous implant tests showed that low concentrations of GO scaffold enhances cell in-growth and is highly biodegradable, whereas high concentrations of GO coating resulted in adverse biological effects. Consequently, scaffolds modified with a suitable concentration of GO are useful as a bioactive material for tissue engineering [32].

The behaviour of Zinc Oxide porous thin films and ZnO thin films coated with GO in Simulated Body Fluid have been investigated in order to study the bioactivity and biodegradation of both materials. The main interest falls on the possibility of using this material as a drug delivery system.

2.4 Hydroxyapatite

Hydroxyapatite (HAp) is a material belonging to the calcium phosphate ceramics. HAp exhibits an excellent biocompatibility and osteogenic potential to promote tissue adhesion and bone growth. Therefore, its formation is a symbol of bioactivity since this material has been studied as a biocompatible material for the reconstruction and filling of bone tissue. The composition of HAp, Ca10(PO4)6(OH)2, closely resembles the one of the mineral component of native bone, i.e. biological apatite, a calcium deficient, carbonate-substituted non-stoichiometric hydroxyapatite [33]. A nanocrystalline structure and a rod-like morphology are two further distinct features that contribute to its unique biological functionality under physiological conditions [33].

The most widely used hydroxyapatite is porous sintered because it can be easily invaded by osteoblasts but, due to the fragility of this component, its application focuses on the coating of metals or in composite materials as a filler in in plastics, glasses and ceramics [34].

One of the main characteristics of this biomaterial is the calcium-phosphorus molar ratio since the lower the ratio, the higher the acidity and solubility of the samples, as well as being a factor related to the mechanical properties of the material. The pure HAp phase has a Ca / P molar ratio of 1.67 [35].

An important characteristic of hydroxyapatite is its stability when compared to other calcium phosphates. Thermodynamically, hydroxyapatite is the most stable calcium phosphate compound under physiological conditions of temperature, pH and composition of the body fluids.

One of the disadvantages of this biomaterial is that it does not inhibit the formation of bacteria, presenting a low antimicrobial activity.

A material is considered bioactive if it has a positive interaction with or effect on any cell tissue in the human body. Bioactivity is often meant as the formation of calcium phosphate deposits on the surface of objects placed in simulated body fluid (SBF). The presence of silanol groups and the textural properties of the bioactive material, such as porosity and pore volume, seem to play an important role in the formation a HAp layer during the immersion in SBF.

As it is extensively explained in Paragraph 3.3, SBF is defined as an acellular, protein-free solution with ion concentrations approximately equal to those of human blood plasma. The nucleating capacity of a biomaterial can be observed by immersing it in SBF. It has been suggested that the nucleation of calcium/phosphates mimics the initial mineralization of bone on the implant surface. So, as HAp is a material belonging to calcium phosphates ceramics, its precipitation is symbol of bioactive behaviour.

The present work aims to study the capacity of porous ZnO thin films precipitation of apatite layers by soaking them with SBF solution.

2.5 Rhodamine-β

Rhodamine-β is a chemical compound and a dye. It is often used as a tracer dye within water to determine the rate and direction of flow and transport. Rhodamine-β dyes fluoresce and can thus be detected easily and inexpensively with instruments called fluorimeters. Rhodamine-β dyes are used extensively in biotechnology applications such as fluorescence microscopy, flow cytometry and fluorescence correlation spectroscopy.

In this thesis work Rhodamine-β has been used as a dye molecule for studying the capacity of porous ZnO thin films in uptaking and releasing molecules.

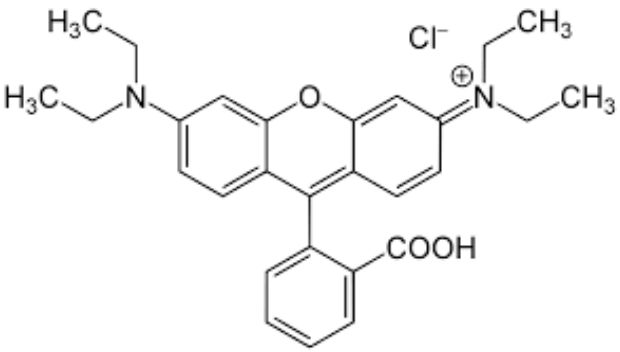

Figure 4: Rhodamine-β chemical structure

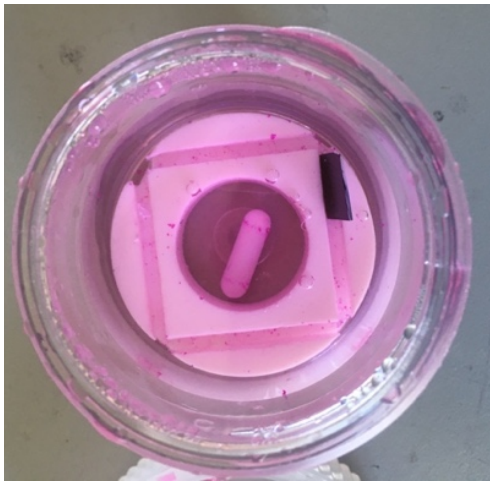

Figure 5: Sample soaked in Rhodamine-B for the uptake experiment

Chapter 3. Materials and methods

In this chapter the methods for obtaining ZnO samples and the GO coating are described, as well as, the composition of SBF solution and the medium for cell culture. There is also an explication of all the characterization setups used and the uptake/release experiment done using Rhodamine-B as a tracer dye.

3.1 Synthesis of porous zinc oxide structures by RF sputtering

Concerning the preparation of ZnO samples, this was carried out by a combination of both physical vapour deposition method, named sputtering, and a final thermal treatment. The preparation of the samples by sputtering is carried out with a deposition system available at the DISAT, which uses a RF magnetron sputtering monotarget system. The deposition process takes place in a cylindrical stainless steel chamber, equipped with a single 4" circular cathode on which the target is clamped, facing downwards. Substrates are placed in the lower part of the reactor, facing upwards toward the target. These technical features guarantee the deposition of uniform and homogeneous coatings on the substrate area.

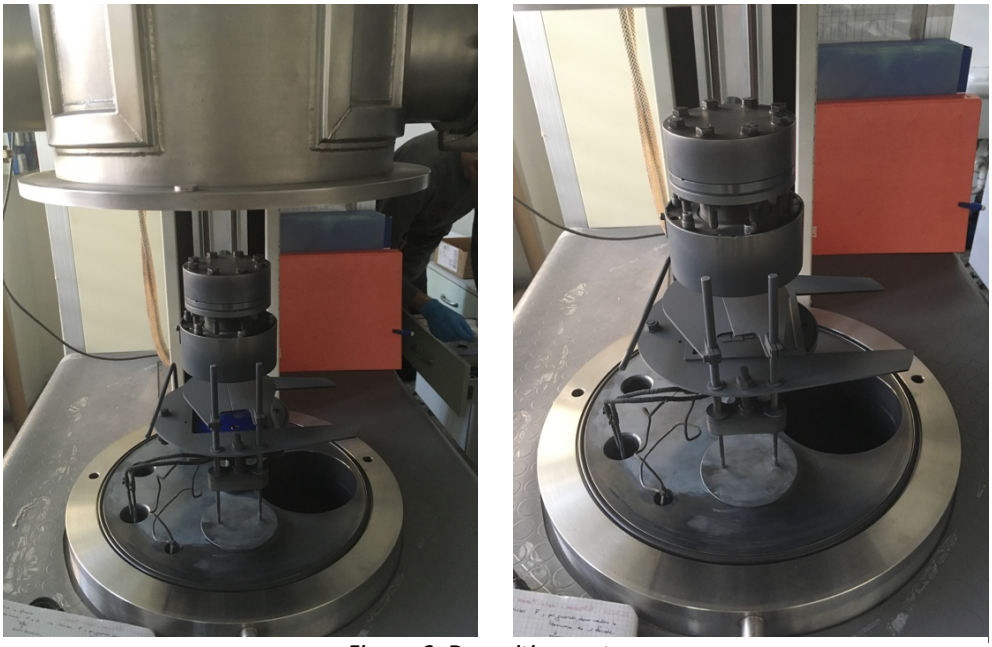

Figure 6: Deposition system

A RF signal generator, operating at a working frequency of 13.56 MHz, and a matching network, needed to adjust the reflected power down to zero, are respectively used to supply and maximize the signal power provided to the cathode. Sputtering deposition of materials requires suitable vacuum conditions before starting the deposition, granting an environment clean from contaminations and from residues such as oxygen and moisture. In our case, these are obtained by a two-stage pumping system, made by a rotary and a turbo molecular pumps connected in series, allowing to reach pressures as low as 10^{-7} Torr [6].

The properties of sputtered ZnO thin films are known to depend on deposition parameters such as RF power, pressure, substrate temperature and gas atmosphere.

So, in this work, ZnO thin films were deposited by RF sputtering on Si (1 0 0) substrates. First, Si substrate was diced into 1 cm x 1 cm pieces. Secondly, those substrates were washed in acetone and ethanol. For each solvent the samples were washed in 50 ml of the corresponding solvent in ultrasound bath for 10 min, then washed with clean solvent and finally dried under nitrogen flow. Thirdly, the deposition process takes place, using the parameters mentioned in *Table 1*. The main reason of using these parameters is that by using them, the obtainment of particular nanoporous structure of ZnO thin films was allowed. Finally, a thermal oxidation was done at 380ºC during 120 min performed in ambient air using a muffle furnace in order to oxidize the Zn layer and to obtain the conversion of the Zn film into ZnO nanostructured layers.

Target	Base Vacuum [Torr]	T [ºC]	Ar flow [sccm]	Pressure [mTorr]	RF power [W]	Deposition time [min]
Zn	$1{,}7\text{x}10^{-7}$	21	10	5	30	240

Table 1: Deposition process parameters

Figure 7: Zn samples after sputtering

3.2 Synthesis and deposition of graphene oxide flakes on porous ZnO structures by drop-casting method

The coating of GO flakes has been fabricated by drop casting method. GO dispersion in water with different concentrations of 0.1 mg/mL, 0.5 mg/mL, and 1 mg/mL was obtained using a modification of the Hummers method [36]. The average lateral size of the GO sheets was on the order of a few to few tenths of micrometers. For each concentration, a droplet of the GO solution with a fixed volume of 50 µL was drop-casted on the surface of each ZnO sample. Then, each sample was air-dried overnight, with the twofold aim of promoting water evaporation and adsorption of the GO flakes to the ZnO surface, hence forming a continuous GO layer.

At the beginning the preparation of three samples coated with different GO concentrations (0.1, 0.5 and 1 mg/ml respectively) was done but, from FESEM analyses we decided to use the 0.5 mg/ml sample since showed a better uniform and homogeneous coverage of the ZnO surface.

For the 0.5 mg/mL GO solution, drop-casting was performed on six ZnO samples, which were then soaked in SBF. The GO-coated ZnO samples were collected from the SBF solution after 5h, 1 day, 3 days, 1 week, 2 weeks and 3 weeks.

3.3 Bioactivity and biodegradation assays using Simulated Body Fluid and medium for cells culture (eMEM)

Simulated body fluid (SBF)

Simulated body fluid (SBF) is a solution which has ions concentrations nearly equal to those of human blood plasma and is buffered at pH 7.4 at 36.5 ºC.

Ion	Simulate Body Fluid	Blood plasma
Na^+	142.0	142.0
K^+	5.0	5.0
Mg^{2+}	1.5	1.5
Ca^{2+}	2.5	2.5
Cl^-	148.8	103.0
HCO^{3-}	4.2	27.0
HPO_4^{2-}	1.0	1.0
SO_4^{2-}	0.5	0.5

Table 2: Comparison between ion concentration in SBF and in human blood plasma

For obtaining this solution one litre polyethylene bottle was filled with 500ml of ion exchanged and distilled water and a magnetic stirrer into it for dissolving the reagents added in the following order:

Order	Reagent	Amount
1	NaCl	7.996 g
2	$NaHCO_3$	0.350 g
3	KCl	0.224 g
4	$K_2HPO_4 \cdot 3H_2O$	0.228 g
5	$MgCl_2 \cdot 6H_2O$	0.305 g
6	1M-HCl	40 mL
(About 90 % of total amount of HCl to be added)		
7	$CaCl_2$	0.278 g
8	Na_2SO_4	0.071 g
9	$(CH_2OH)_3CNH_2$	6.057 g

Table 3: Reagents for preparing SBF solution

Once all the reagents were dissolved, the temperature was adjusted at 36.5ºC with a water bath and adjusted the pH at 7.40 by stirring the solution and titrating 1N·HCl solution. After that, a transfer of the solution to a volumetric glass flask and an adjustment of the total volume of the solution to one litre by adding ion exchanged and distilled water and shaking the flask at 20ºC, were done. [37]
Finally, the bottle was stored in the refrigerator at 5ºC and used within one month from the production.

Each of the samples were placed in different plastic flasks with SBF into the orbital shaker (for simulating the body fluids movement) at 37ºC, during the time corresponding each sample had to be. Each time a sample was removed from the SBF solution, it was cleaned with distilled water and dried at room temperature.

The refresh of the solution was done to some samples every 2 days, which means that there was a change of the SBF solution. It was done in order to study the HAp precipitation on the sample surface. In contrast, to study the biodegradation of the samples there were others without refresh thus, it was easier to investigate

the release of ions from the sample to the solution. The bioactivity analyses were done according to the Kokubo Test [38].

The orbital shaker used was Excella^{TM} E24/ Temperature-Controlled Benchtop Shakers and the parameters of shaking were a continuous shaking at 160 rpm with a temperature of 37ºC.

Figure 8: Orbital Shaker

Cell culture medium (eMEM)

Cell culture medium is a solution designed to support the growth of cells under controlled conditions. Even cell culture conditions can vary for each cell type, artificial environments consist of a suitable vessel with substrate or medium that supplies the essential nutrients and regulates the physico-chemical environment. The eMEM used in this thesis work have been done by following M4655 Sigma-Aldrich instructions described in Table 4.

	M4655
	[1×]
COMPONENT	g/L
Inorganic salts	
$CaCl_2$	0.265
$MgSO_4$ (anhydrous)	0.09767
KCl	0.4
KH_2PO_4	—
$NaHCO_3$	2.2
NaCl	6.8
Na_2HPO_4 (anhydrous)	—
NaH_2PO_4 (anhydrous)	0.122
$NaH_2PO_4 \cdot H_20$	—
Amino acids	
L-Alanine	—
L-Alanyl-L-Glutamine	—
L-Arginine • HCl	0.126
L-Asparagine • H_20	—
L-Aspartic acid	—
L-Cystine • 2HCl	0.0313
L-Glutamic acid	—
L-Glutamine	0.292
Glycine	—
L-Histidine • HCl • H_20	0.042
L-Isoleucine	0.052
L-Leucine	0.052
L-Lysine • HCl	0.0725
L-Methionine	0.015
L-Phenylalanine	0.032
L-Proline	—
L-Serine	—
L-Threonine	0.048
L-Tryptophan	0.01
L-Tyrosine • 2Na • $2H_20$	—
L-Tyrosine	0.0519
L-Valine	0.046
Vitamins	
Choline chloride	0.001
Folic acid	0.001
myo-Inositol	0.002
Niacinamide	0.001
D-Pantothenic acid • ½Ca	0.001
Pyridoxal • HCl	0.001
Riboflavin	0.0001
Thiamine • HCl	0.001
Other	
D-Glucose	1.0
Phenol red • Na	0.011
Add	
L-Glutamine	—
$NaHCO_3$	—

Table 4: Quantities of the components needed for obtaining M4655 eMEM

To this eMEM, there has been added 10% of Fetal Bovine Serum (FBS) with the following composition (Table 5).

Composition of FBS

Component	Average	Range
Endotxins (ng/ml)	0.35	0.01 - 10.0
Glucose (mg/ml)	1.25	0.85 - 1.81
Protein (mg/ml)	38	32 - 70
Albumin (mg/ml)	23	20 - 36
Hemoglobine (µg/ml)	113	24 - 181
Bilirubin, total (µg/ml)	4	3 - 11
Bilirubin, direct (µg/ml)	2	0 - 5
Urea (µg/ml)	160	140 - 200
Urate (µg/ml)	29	13 - 41
Creatinin (µg/ml)	31	16 - 43
Insulin (µU/ml)	10	6 - 14
Cortisol (ng/ml)	0.5	0.1 - 23
Growth hormone (ng/ml)	39.0	18.7 - 51.6
Parathormone, PTH (ng/ml)	1.72	0.085 - 6.18
Triiodothyronine, T3 (ng/ml)	1.2	0.56 - 2.23
Thyroxine, T4 (ng/ml)	0.12	0.08 - 0.16
Thyroid-stimulating hormone, TSH (ng/ml)	1.22	0.2 - 4.5
Follicle-stimulating hormone, FSH (pg/ml)	95	20 - 338
Testosterone (pg/ml)	400	210 - 990
Progesterone, P4 (pg/ml)	80	3 - 360
Prolactin = Luteotropic hormone, LTH (pg/ml)	176	20 - 500
Luteinizing hormone, LH ?? (pg/ml)	8	1,2 - 18
Prostaglandin E (ng/ml)	5.9	0.5 - 30.5
Prostaglandin F (ng/ml)	12.3	3.8 - 42.0
Vitamine A (ng/ml)	90	10 - 350
Vitamine E (ng/ml)	1.1	1 - 4.2
Cholesterol (µg/ml)	310	120 - 630
Lactate-dehydrogenase, LDH (mU/ml)	864	260 - 1,215
Alkaline Phosphatase (mU/ml)	255	110 - 352
Aspartate-Aminotransferase, ASAT (mU/ml)	130	20 - 200
Sodium, Na^+ (µeq/ml)	137	125 - 143
Potassium, K^+ (µeq/ml)	11.2	10.0 - 14.0
Calcium, Ca^{2+} (µeq/ml)	6.75	6.30 - 7.15
Chloride, Cl^- (µeq/ml)	103	98 - 108
Phosphate, P_i (µg/ml)	98	43 - 114
Selen (µg/ml)	0.026	0.014 - 0.038
pH	7.40	7.20 - 7.60

from Lindl, T. (2002): "Zell- und Gewebekultur". 5th ed. Spektrum Akademischer Verlag, Heidelberg

Table 5: Composition of FBS

Also, with the addition of penicillin-streptomycin at 1%.

TEST	Specification
Appearance (Form)	Liquid
Appearance (Turbidity)	Clear
Osmolality	
Penicillin (U/ml)	10000 - 12000
Potency Streptomycin	10 - 12 mg/ml
Sterility	Pass
Endotoxin Level at 10ml/L	≤ 0.5 EU/ml
Cell Line	Hep-2 Human Cells
Cell Culture Test	≥ 50 %
percent of control	
Expiration Date Period	---------
24 months	

Specification: PRE0.ZQ5.10000014726

Table 6: Composition of penicillin-streptomycin

3.4 Uptake and release Rhodamine-β dye molecule on porous ZnO structures for drug delivery applications experiment preparation

As it is mentioned above, Rhodamine-B is used in this work thesis as a dye molecule for studying the uptake and release of this solution from porous ZnO thin films.

The followed methodology begins with a measurement of UV absorbance of Rhodamine-β each time the experiment have been done for observing the calibration curvature of the solution at that point. Rhodamine-β photodegradation with UV has to be taken in account when doing this experiment as every time the solution was exposed UV light its properties could vary.

Then, for observing the uptake of Rhodamine-β dye molecule on porous ZnO thin films 20ml of Rhodamine-β were put inside a flask with a magnetic stirrer and the sample and leaved it stirring at 600 rpm. As this solution is easily degraded by UV light, covering the flask with aluminium paper was essential. After 1, 2, 3, 4, 5 and 24 hours we collected 100μl of the solution and placed it in the microplate.

100μl of Rhodamine-β and 100μl of water were also collected before the experiment.

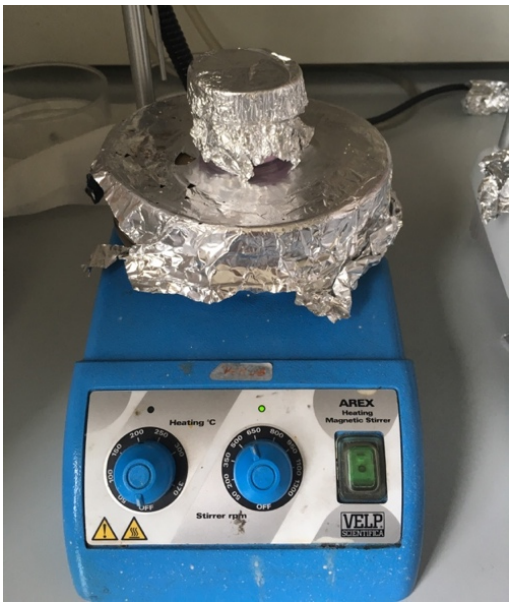

Figure 9: Uptake experiment with Rhodamine-B solution covered with aluminium paper stirring at 600 rpm

For the release experiment, a plastic tube filled with SBF solution and a magnetic stirrer was put it into an experimental setup stirring at 150 rpm, with constant temperature of 37ºC. After 30 min (time estimated for the solution to get the necessary conditions) the sample was placed inside. To evaluate the amount of Rhodamine-β released from the porous ZnO sample, 100μl of the solution at different time points: after 5, 15, 30 minutes, 1, 2, 4 and 6 hours and then after 1, 2 and 3 days, were collected and put into the microplate. As in the uptake experiment, 100μl of SBF solution before the experiment and 100μl of water were also collected.

By using the microplate reader, the amount of Rhodamine-β that have been uptaken from the sample and the amount of Rhodamine-β that have been released to the SBF solution were obtained.

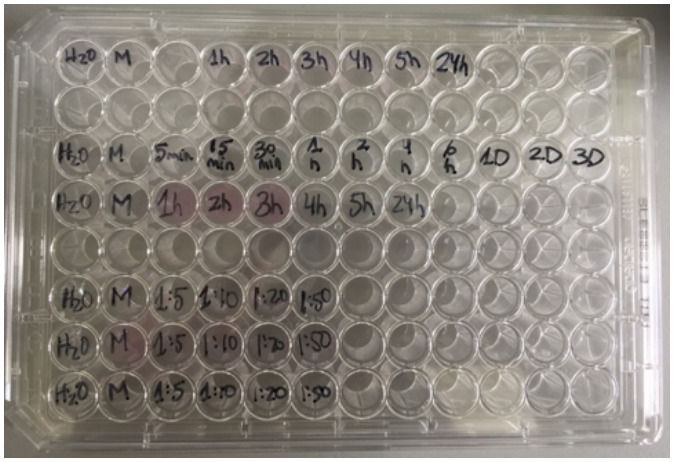

Figure 10: 96-well microplate used for estimating the amount of Rhodamine-B uptaken and released by the ZnO porous samples

3.5 Physico-chemical characterization setups

3.5.1 X-Ray Diffraction (XRD)

X-ray diffraction (XRD) is a method useful to determine the crystallinity of a compound and it is primarily used for:

- Identification of crystalline material
- Identification of different polymorphic forms
- Distinguishing between amorphous and crystalline material
- Quantification of the percent crystallinity of a sample

XRD analysis is based on constructive interference of monochromatic X-rays and a crystalline sample: The X-rays are generated by a cathode ray tube, filtered to produce monochromatic radiation, collimated to be spatially localized, and then directed toward the sample. The interaction of the incident rays with the sample produces constructive interference (and a diffracted ray) when conditions satisfy Bragg's Law ($n\lambda=2d \sin \theta$). This law relates the wavelength of electromagnetic radiation to the diffraction angle and the lattice spacing in a crystalline sample.

The characteristic x-ray diffraction pattern generated in a typical XRD analysis provides a unique “fingerprint” of the crystals present in the sample. When properly interpreted, by comparison with standard reference patterns and measurements, this fingerprint allows identification of the crystalline form.

The result from an XRD analysis is a *diffractogram* showing the intensity of the diffracted beam as a function of the diffraction angles (2θ).

With these measurements there was the expectancy to see clearly the peaks corresponding to ZnO crystalline structure and the HAp peaks if it is precipitated.

The instrument used is shown in *Figure 11*, and consists of a PANalytical X’Pert³ Powder diffractometer of Dipartimento di Scienza Applicata e Tecnologia (DISAT) of Politecnico di Torino. The parameters used were an intensity of 30mA and a tension of 40kV.

Figure 11: PANalytical X’Pert³ Powder

3.5.2 Field-Emission Scanning Electron Microscopy (FESEM)

Field Emission Scanning Electron Microscopy (FESEM) reveals detailed information about the morphology and the composition of materials at magnifications 12x to 900,000x, with virtually unlimited depth of field.

It's principle of operation is based on a field-emission cathode in the electron gun of a scanning electron microscope that provides narrower probing beams at low as well as high electron energy, resulting in both improved spatial resolution and minimized sample charging and damage.

FESEM analyses were performed in order to see the morphology of the sample focusing on calcium and phosphorous structures and its coverage on the surface of the sample.
The instrument used was SUPRA™ 40 (ZEISS) that has been developed as an extremely versatile FESEM capable of delivering high quality imaging solutions for the many demanding applications in the field of nanotechnology. The parameters found in *Table 7* are the characteristics of this instrument.

Nominal resolution at 10kV and WD=2mm	**Acceleration voltage**	**Probe current**	**Magnification**	**Working distance**
1.5nm	0.1 – 30kV	4pA – 10nA	12 – 900,000X	1 – 50mm

Table 7: SUPRA™ 40 (ZEISS) characteristics

The sample holder can host nine stubs. Each stub can contain samples of about 1 cm^2.

Figure 12: SUPRA™ 40 (ZEISS)

3.5.3 Attenuated Total Reflection (ATR) – IR spectroscopy

Mid-Infrared (IR) spectroscopy is an extremely reliable and well recognized fingerprinting method. Most substances show a characteristic spectrum that can be directly recognized. ATR-IR spectroscopy enables measuring all types of samples: solids, liquids and gases.

The ATR principle is based on the ATR crystal that comprises an IR transparent material with a high refractive index and polished surfaces.

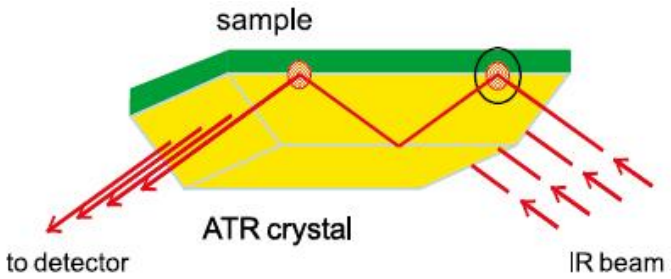

Figure 13: ATR principle

As shown in *Figure 13*, the infrared beam enters the ATR crystal at an angle of typically 45° and is totally reflected at the crystal to sample interface. Because of its wave-like properties, the light is not reflected directly by the boundary surface

but by a virtual layer within the optically less dense sample. The fraction of light reaching into the sample is known as evanescent wave. Its penetration depth depends on the wavelength, the refractive indices of the ATR crystal and the sample, and the angle of the entering light beam. It is typically on the order of a few microns (ca. 0.5 - 3 µm). In the spectral regions where the sample absorbs energy, the evanescent wave is attenuated. After one or several internal reflections, the IR beam exits the ATR crystal and is directed to the IR-detector.

ATR-IR measurements were done in order to study the substances of which our samples are composed and the different impact they cause. ATR-IR spectrum were collected in the range of 4000-400 cm^{-1}, at 2 cm^{-1} resolution. 64 scans were accumulated for each spectrum on a Nicolet 5700 FTIR spectrometer (Thermofisher) equipped with a room temperature working deuterated triglycine sulphate (DTGS) detector and a diamond crystal accessory. In *Figure 14* there is an example of ATR-IR spectrum instrument.

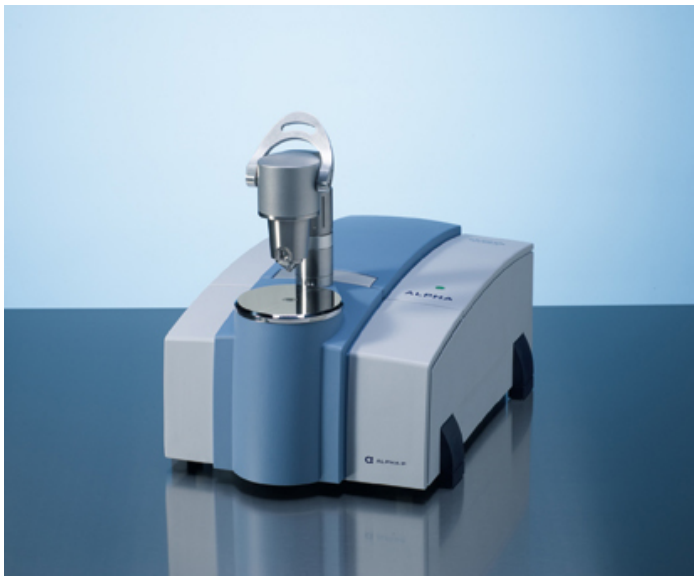

Figure 14: ATR-IR spectrometer

3.5.4 Energy-Dispersive X-Ray Spectroscopy (EDS) maps

Energy-dispersive X-ray spectroscopy (EDS) is an analytical technique used for the elemental analysis and chemical characterization of a sample. It relies on an interaction of incident primary electron and the consequent emission of X-ray from the sample. Its characterization capabilities are due to the principle that each element has a unique atomic structure allowing a unique set of peaks on its electromagnetic emission spectrum.

The number and energy of the X-rays emitted from a specimen can be measured by an energy-dispersive spectrometer. As the energies of the X-rays are characteristic of the difference in energy between the two shells and the atomic structure of the emitting element, EDS allows the elemental composition of the specimen to be measured.

Four primary components of the EDS setup are:

- the excitation source (electron beam or x-ray beam)
- the X-ray detector
- the pulse processor
- the analyser

In this thesis, EDS maps have been carried out with the twofold aim of estimating the chemical composition of the samples and the distribution of the elements on the samples surface. The setup used in this thesis work consisted of a desktop SEM Phenom XL equipped with EDS analyser. Each EDS map was acquired on a 1000X SEM image, with the parameters described in *Table 8.*

Map resolution	Acquisition time per pixel	Number of scans
128 pixel	20ms	1

Table 8: EDS maps parametres

3.5.5 Inductively Coupled Plasma (ICP) mass spectrometry

ICP-MS is an analytical technique used for elemental determinations that has many advantages such as atomic absorption, optical emission spectrometry, high throughput and detection limits for most elements equal to or better than other standard methods for element identification.

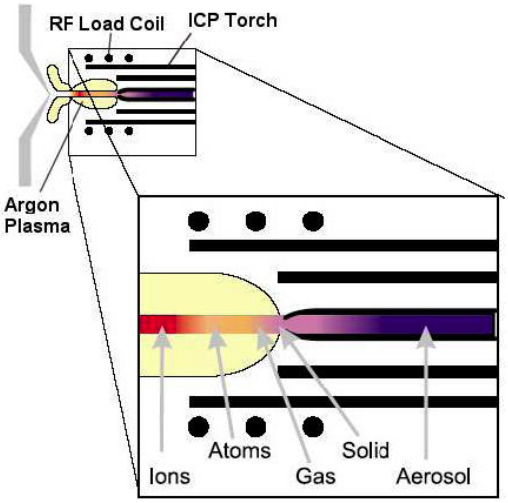

Figure 15: ICP Torch showing the fate of the sample

An ICP-MS combines a high-temperature ICP (Inductively Coupled Plasma) source with a mass spectrometer. The ICP source converts the atoms of the elements in the sample into ions. These ions are then separated and detected by the mass spectrometer.

The sample is typically introduced into the ICP plasma as an aerosol, either by aspirating a liquid or dissolved solid sample into a nebulizer or using a laser to directly convert solid samples into an aerosol. Once the sample aerosol is introduced into the ICP torch, it is completely dissolved and the elements in the aerosol are converted first into gaseous atoms and then ionized towards the end of the plasma.

Once the elements in the sample are converted into ions, they are then brought

into the mass spectrometer via the interface cones. The interface region in the ICP-MS transmits the ions traveling in the argon sample stream at atmospheric pressure into the low pressure region of the mass spectrometer. This is done through the intermediate vacuum region created by the two interface cones, the sampler and the skimmer.

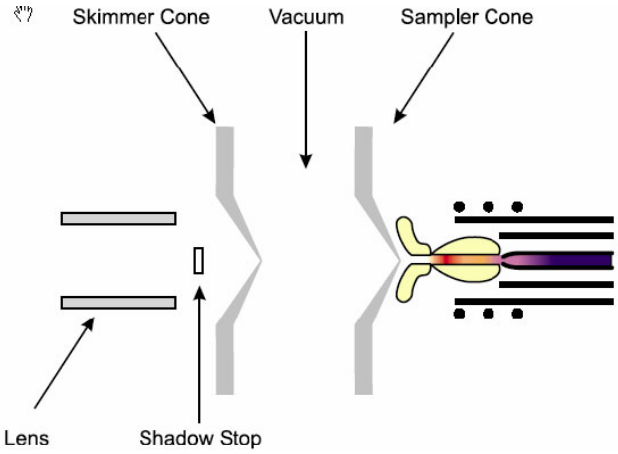

Figure 16: Interface region of an ICP-MS

The ions from the ICP source are then focused by the electrostatic lenses in the system.

Once the ions enter the mass spectrometer, they are separated by their mass-to-charge ratio. The most commonly used type of mass spectrometer is the quadrupole mass filter.

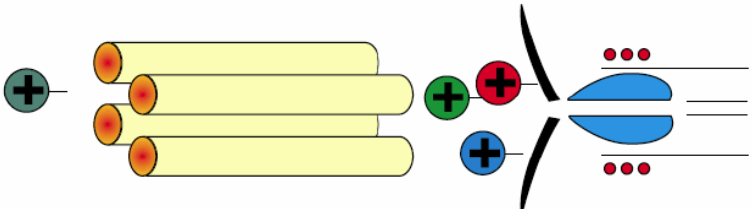

Figure 17: Schematic of quadrupole mass filter

The ability to filter ions on their mass-to-charge ratio allows ICP-MS to supply isotopic information, since different isotopes of the same element have different masses. [39]

In this thesis work an Inductively Coupled Plasma Mass Spectrometry (ICP-MS) (mod. 7500cc, AGILENT TECHNOLOGIES, Milan, Italy) was used, with the aim of finding how changed are the ions of the solution after the samples of porous ZnO and ZnO coated with GO have been soaked there.

3.5.6 Microplate reader

Microplate readers are instruments used to detect biological, chemical or physical events of samples in microtiter plates. They are widely used in research, drug discovery, bioassay validation, quality control and manufacturing processes in the pharmaceutical and biotechnological industry and academic organizations.

The most common microplate format used in academic research laboratories or clinical diagnostic laboratories is 96-well (8 by 12 matrix) with a typical reaction volume between 100 and 200 µL per well. Common detection modes for microplate assays are absorbance, fluorescence intensity, luminescence, time-resolved fluorescence, and fluorescence polarization.

Figure 18:Microplate Reader

The one used in this thesis work was a Multiskan™ GO Microplate Spectrophotometer from Thermo Fisher Scientific, that analyses the most common microplate format 96-well (8 by 12 matrix) detecting the UV absorption of the specimens introduced, as reported in *Figure 10* with a typical reaction volume of 100 µL.

3.5.7 Fluorescence Microscopy

Fluorescence microscopy is a technique for acquiring microscopic images of samples (often biological materials) using fluorescence within the sample, which is usually excited with a sharply focused diffraction-limited laser beam.

The focus of the laser beam is raster scanned through the simple, and the fluorescent light excited in the sample is collected with some optics and monitored with a photodetector. Residual laser light can be eliminated with an optical filter before the detector.

The fluorescence microscope is usually operated with a computer (a PC or a laptop), which controls the scan, records the fluorescence intensities, and finally generates, processes and stores the obtained images.

The fluorescence can originate from molecules which occur naturally in the sample, or from dye molecules which are introduced during sample preparation.

In the simplest form of fluorescence microscopy, the laser is operated continuously, and its wavelength is chosen to be in an absorbing spectral region of the fluorescent molecules, which can therefore be excited with single-photon absorption.

As mentioned above, fluorescence microscopy is mostly used for biological samples. It is currently investigated in which form fluorescence microscopy can be used e.g. for the detection of cancer. It is also useful for imaging living cells [40].

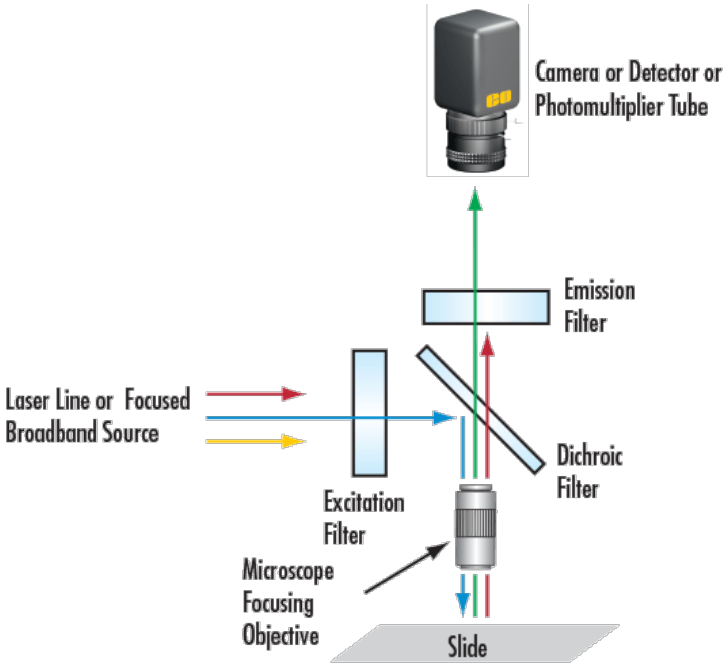

Figure 19: Basic Optical Filtering Arrangement for Fluorescence Microscopy

Chapter 4. Results and discussion

For studying the interaction of porous ZnO thin films with simulated body fluid (SBF) and medium for cells culture (eMEM), an investigation of the samples soaked for different periods of time was done in terms of their morphology, crystal structure and chemical composition. The above mentioned characteristics were investigated by means of Field-Emission Scanning Electron Microscopy (FESEM) measurements, x-Ray Diffraction (XRD), Attenuated Total Reflection (ATR) and Energy Dispersive X-ray Spectroscopy (EDS), respectively.

For investigating the possible drug delivery applications, the capacity of porous ZnO samples to uptake and release Rhodamine-B was studied.

The results of this thesis work are structured in 4 sections, the first concerning the *in-vitro* evaluation of bioactivity and biodegradation properties of porous ZnO samples soaked in SBF, the second concerning the same evaluation for the ZnO samples coated with GO, the third concerning the in-vitro evaluation of cell culture formation on porous ZnO samples soaked in eMEM, and finally a fourth section in which there are reported the results concerning the ability of ZnO samples to uptake and release Rhodamine-B dye molecule.

For the first two sections, the analyses mentioned above were done on 12 samples of ZnO and to 6 samples of ZnO coated with GO soaked in SBF solution. In the third section, the analyses were done on 5 samples soaked in medium for cells culture.

Concerning the ZnO samples soaked in SBF solution, there are 7 samples without SBF refreshing, i.e., the SBF solution was not changed during the experiments and 5 samples with refresh, meaning that change of the SBF solution with a fresh one was performed every 2 days.

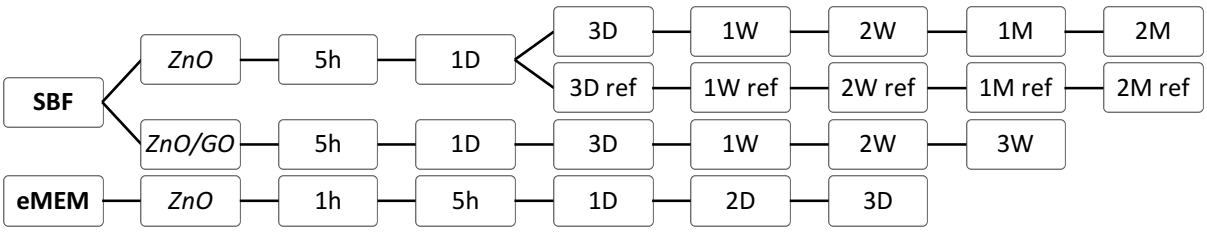

Figure 20: Diagram resuming sample's tests and time steps, where h: hours, D: days, W: weeks, M: month

The experiment performed in SBF was done until 2M soaking time because the result desired are appreciable after long periods of time while, in the experiment performed in eMEM, the typical time needed to well appreciate cell culture structures formation is 3D.

4.1 *In-vitro* evaluation of bioactivity and biodegradation properties of porous ZnO structures soaked in SBF

Bioactivity and biodegradation properties were studied with the above mentioned characterization setups. The results are divided into sections, according to the physicochemical characterization method.

4.1.1 Attenuated Total Reflection (ATR)

ATR is an effective method to reveal the composition of specific compounds, represented by the presence of IR absorbance bands for each specific chemical group. In *Figure 21 and Figure 22,* are shown the different ATR spectra obtained from the analyses of all the ZnO samples with refresh and without refresh, respectively.

When soaking porous ZnO samples in SBF solution there is an appreciation of the different phosphates bands, one positioned between 969 and 1190 cm^{-1} and corresponding to v_3 mode, a second one at 960 cm^{-1} corresponding to v_1 mode, and another between 550 and 680 cm^{-1} corresponding to v_4 mode. The presence of OH groups is also noticed between those two bands. The amide I band is also present with the corresponding band, located in the range 1600 – 1700 cm^{-1} and with a maximum at 1650 cm^{-1} [41].

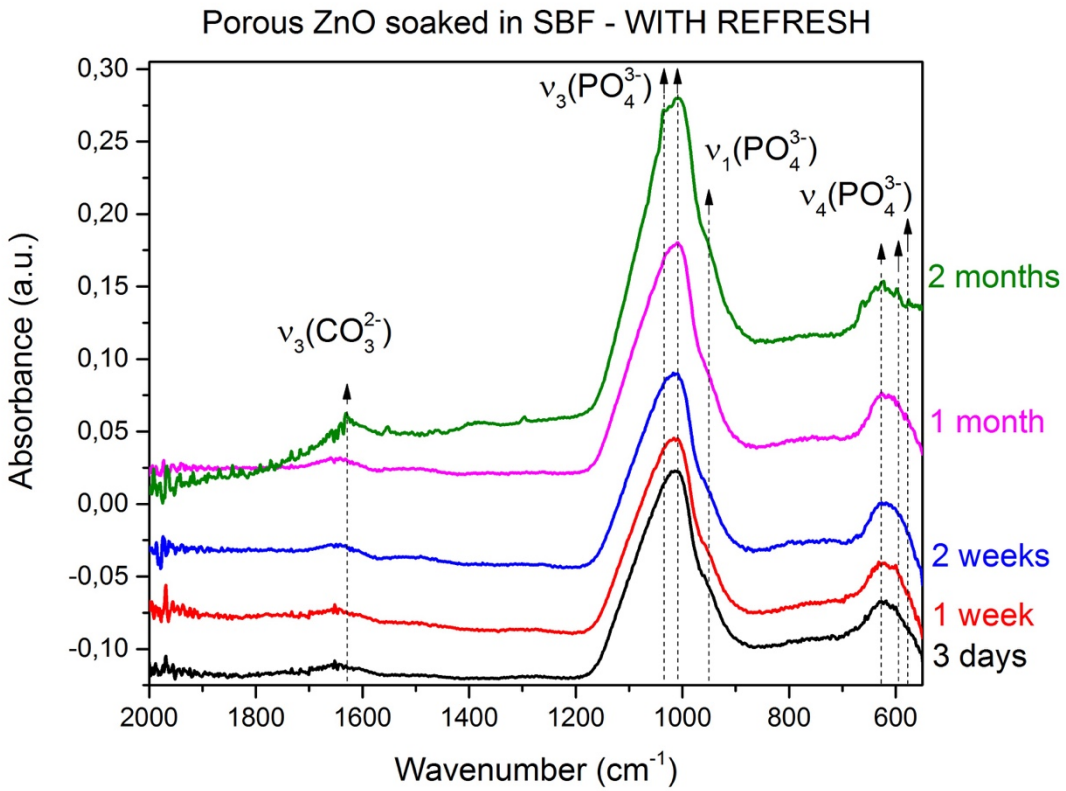

Figure 21: ATR spectra of ZnO samples soaked in SBF with refresh

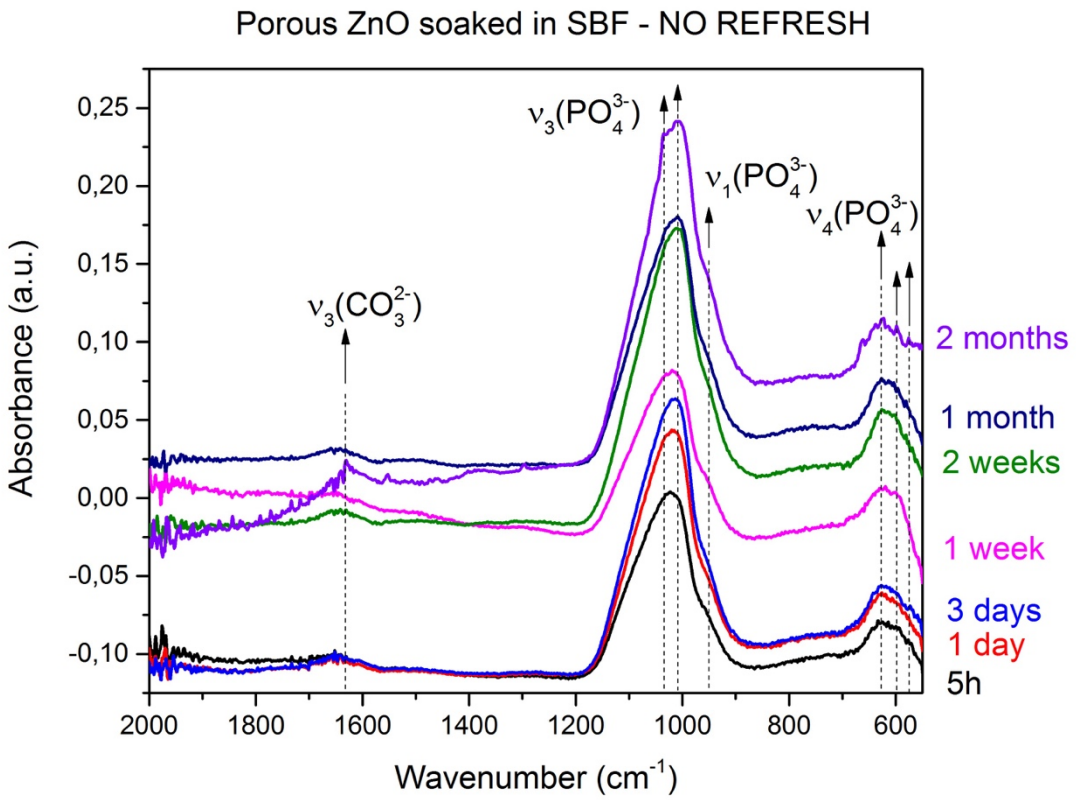

Figure 22: ATR spectra of ZnO samples soaked in SBF without refresh

4.1.2 Energy-Dispersive X-Ray Spectroscopy (EDS)

The EDS technique has been used for obtaining a map of the chemical composition of the samples.

In *Figure 23* and *Figure 24* there is the evolution of the EDS maps among the soaking time in SBF with refreshing and without refreshing the SBF solution, respectively. After soaking the sample for 5h, a fast precipitation of P from SBF solution is obtained. By increasing the soaking time, i.e., after 1D, Ca precipitation also started to appear (purple pixels). Also, in the last EDS map, corresponding to the 2M with refresh sample, we can find a little contribution of chlorine.

Figure 25 and *Figure 26,* show the evolution of Ca and P content versus the soaking time. It is well visible that both Ca and P concentrations increases with time (both with and without refreshing the SBF solution). Moreover, the Ca/P stoichiometry ratio slightly increases by increasing the soaking time.

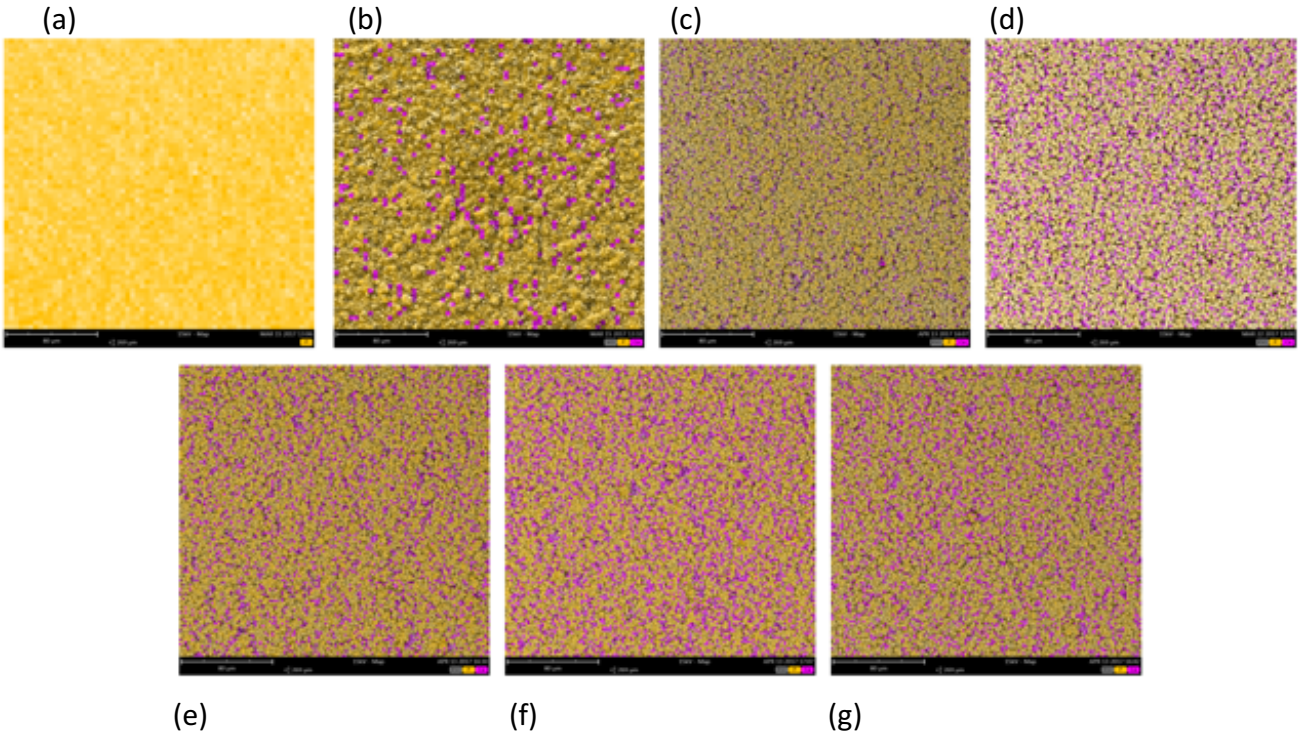

Figure 23: EDS map of the ZnO samples soaked in SBF without refresh for: (a) 5h, (b) 1D, (c) 3D, (d) 1W, (e) 2W, (f) 1M, (g) 2M

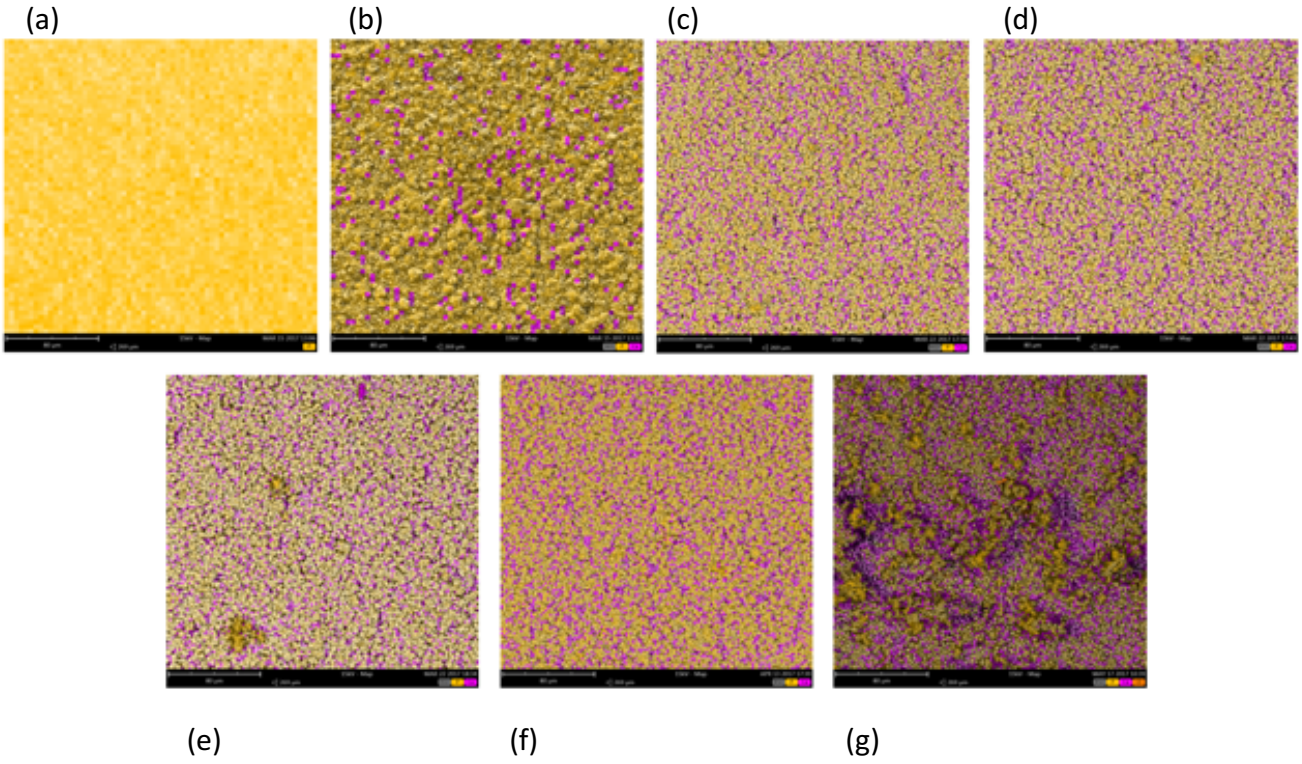

Figure 24: EDS map of the ZnO samples soaked in SBF with refresh for: (a) 5h, (b) 1D, (c) 3D, (d) 1W, (e) 2W, (f) 1M, (g) 2M

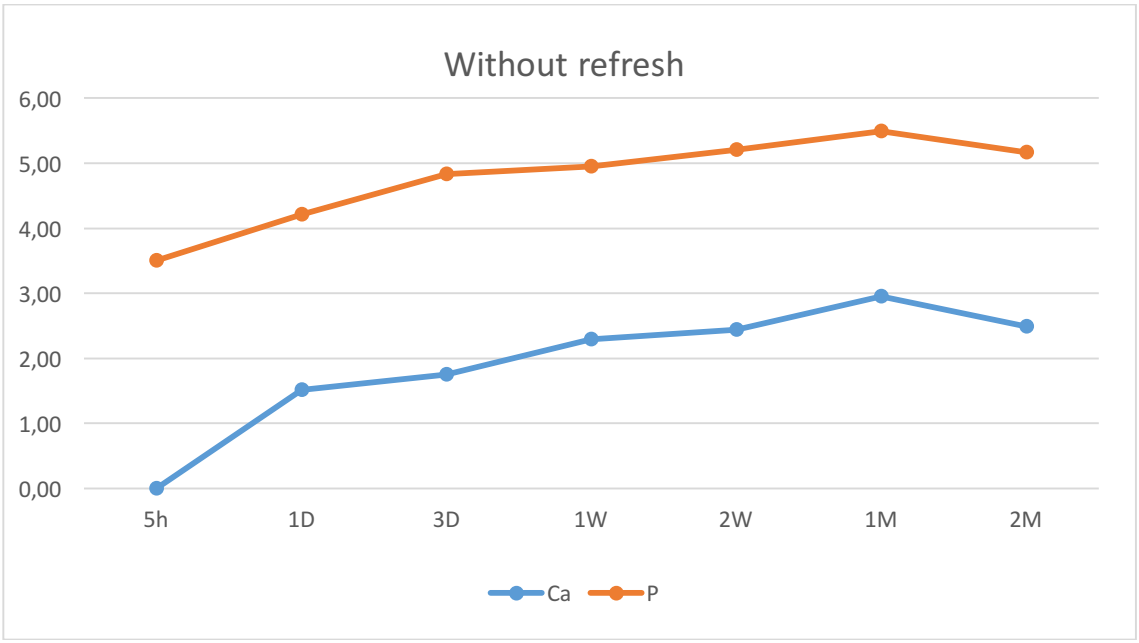

Figure 25: Evolution of Ca and P versus the soaking time without refreshing the SBF solution

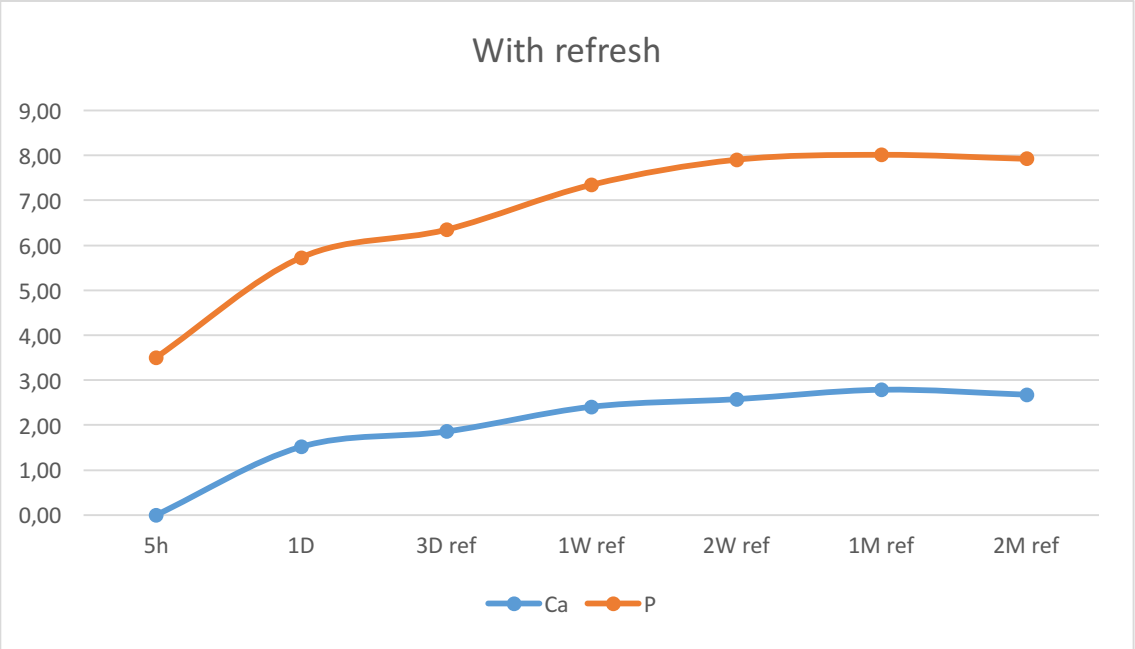

Figure 26: Evolution of Ca and P versus the soaking time when refreshing the SBF solution

With the data obtained, we found that, by increasing the soaking time in the SBF solution, the amount of Calcium (Ca) and Phosphorous (P) increases accordingly.

If we only contemplate those analyses, we can not affirm that hydroxyapatite is precipitated on the surface of the samples, since Ca/P stoichiometry ratio of 1.67 should be obtained. But, as Ca precipitation is observed, it is likely HAp to be formed. Moreover, it is mandatory to take into account that part of the P is chemically bound to Zn, and participating in the formation of zinc phosphates.

4.1.3 Field-Emission Scanning Electron Microscopy (FESEM)

The morphology of the investigated samples was investigated by FESEM analyses.

The following images show the evolution of the samples at increasing time in SBF. *Figure 27* and *Figure 28* show the FESEM images for the samples soaked in SBF for 5 hours and 1 day, respectively, acquired with different magnifications. The following three (*Figure 29, Figure 30* and *Figure 31*) correspond to the samples soaked in SBF for 3 days, 1 week and 2 weeks, respectively. When applicable, the left panel of the FESEM image refers to the ZnO sample soaked in SBF without refresh, while the right part shows the ZnO sample soaked with refresh of SBF, for the same soaking time.

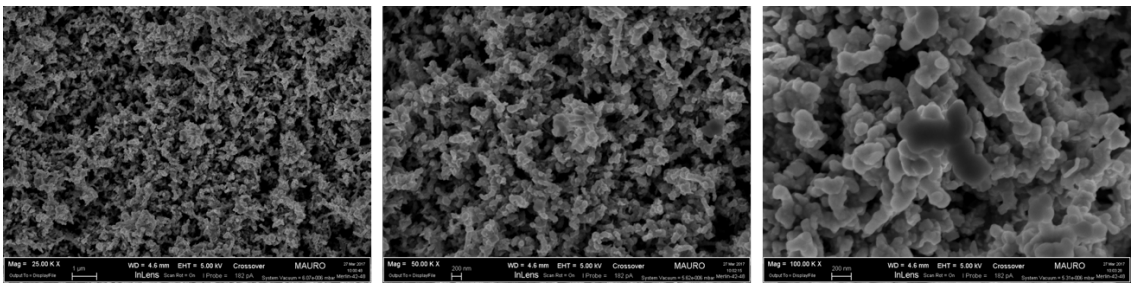

Figure 27: FESEM image of ZnO soaked in SBF for 5h. 25,00 KX left, 50,00 KX middle, 100,00 KX right

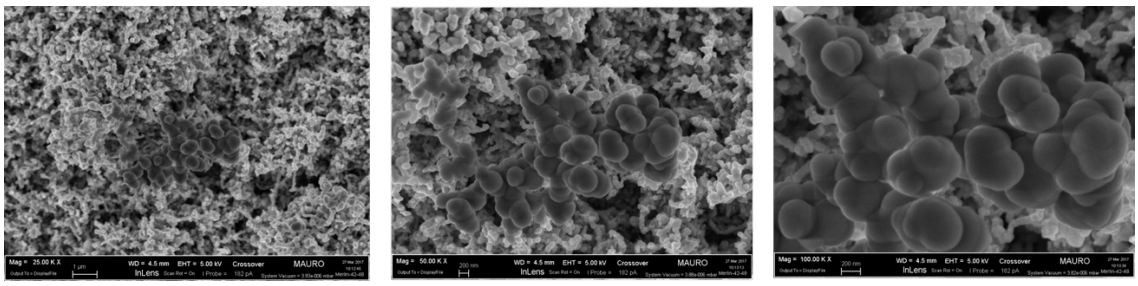

Figure 28: FESEM image of ZnO soaked in SBF for 1D. 25,00 KX left, 50,00 KX middle, 100,00 KX right

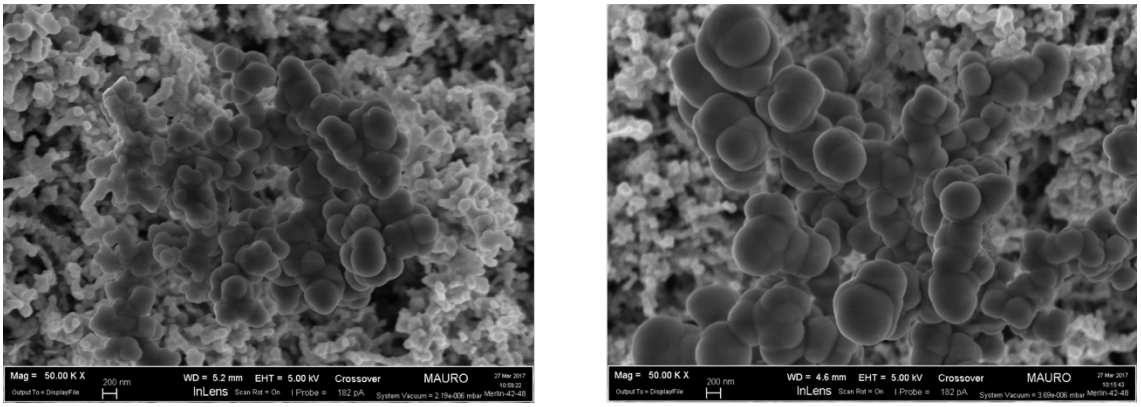

Figure 29: FESEM image of ZnO soaked in SBF for 3D. 50,00 KX without refresh left, 50,00 KX with refresh right

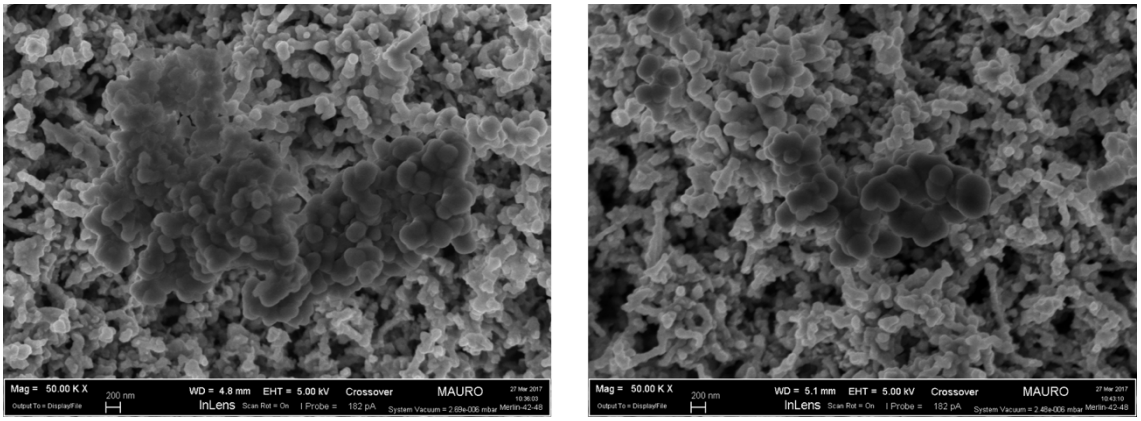

Figure 30: FESEM image of ZnO soaked in SBF for 1W. 50,00 KX without refresh left, 50,00 KX with refresh right

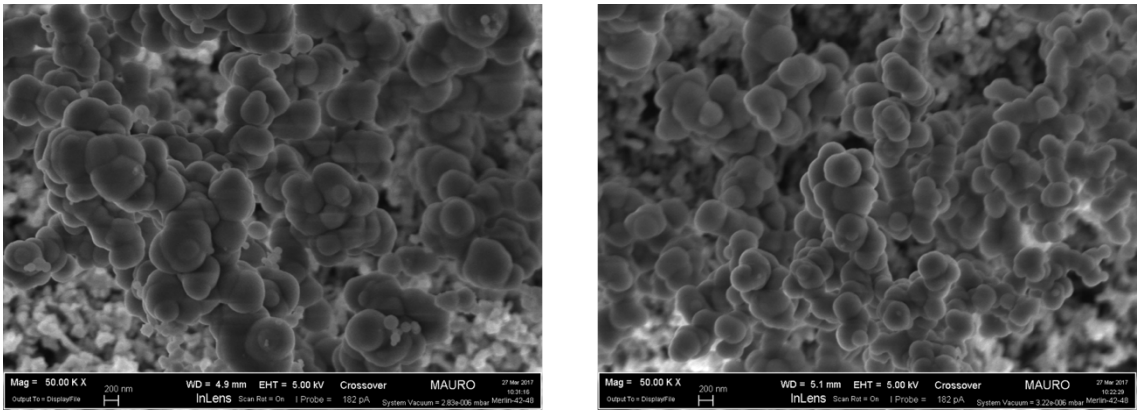

Figure 31: FESEM image of ZnO soaked in SBF for 2W. 50,00 KX without refresh left, 50,00 KX with refresh right

Finally, in *Figure 32* there is a comparison between the sample after 1M and the sample after 2M (both samples were with refreshing the SBF solution).

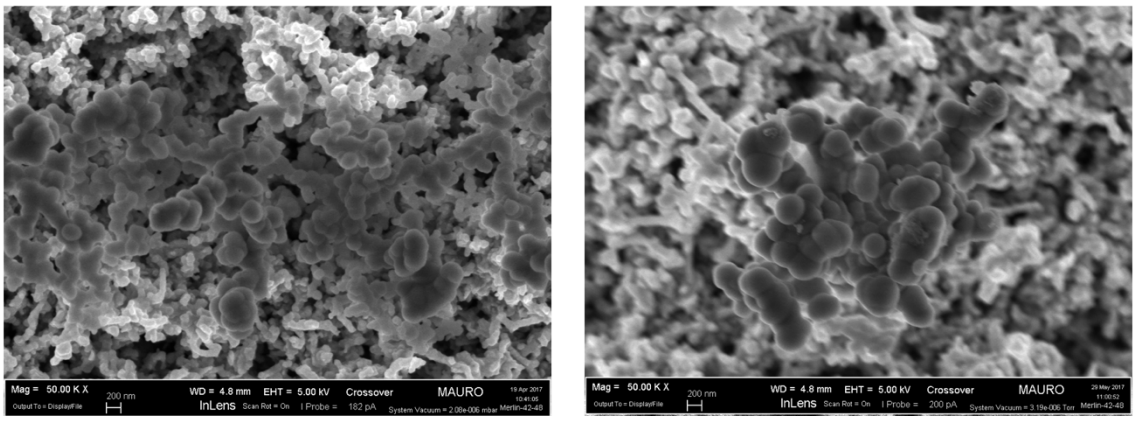

Figure 32: Comparison between 1M sample (left) and 2M sample (right)

The results of the ZnO samples soaked in SBF solution show that a phase of calcium phosphate (biological apatite) can grow efficiently over a porous ZnO thin film, by incubating it in a solution with ionic composition similar to that of blood plasma. Calcium phosphate nucleation started from the first day. As the immersion time increases calcium phosphates cover the entire surface. In the samples without refreshing, the appearance of calcium phosphates was observed too. No appreciable differences in the dimension of CaP precipitates was generally observed by refreshing the SBF solution.

4.1.4 X-Ray Diffraction (XRD)

XRD was selected as the most suitable method to study the crystal structure of the samples.

XRD analyses have been first carried out on the porous ZnO samples soaked in SBF without refreshing the solution. The different ZnO samples were collected from the SBF solution after 5h, 1 day (1D), 3 days (3D), 1 week (1W), 2 weeks (2W),1 month (1M) and 2 months (2M), respectively. Finally, the XRD patterns of the 5 ZnO samples soaked in SBF by refreshing the solution every 2 days were also investigated (3D-refr, 1W-refr, 2W-refr, 1M-refr, 2M-refr).

Independently of refreshing the SBF solution, the XRD patterns do not show significant differences in the crystal structure of the different ZnO samples soaked in SBF up to 1 month. Until this time point, all of them are characterized by relatively strong ZnO (100), ZnO (002) and ZnO (101) diffraction peaks characteristics of the hexagonal wurtzite ZnO structure. Additional peaks corresponding to the ZnO (102) and ZnO (110) planes have been detected as well, even though with a lower intensity.

The XRD peak position detected for all the porous ZnO samples soaked in SBF are reported in Table 9.

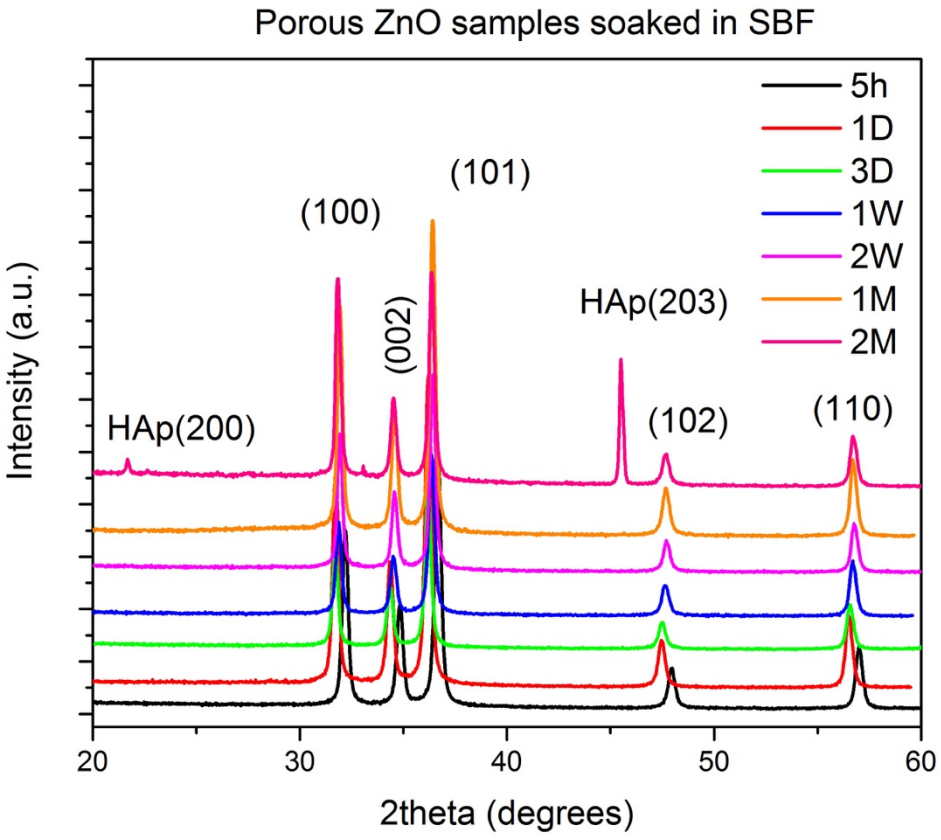

Figure 33: XRD pattern of the porous ZnO samples soaked in SBF

	2θ position						
Sample	**ZnO (100)**	**ZnO (002)**	**ZnO (101)**	**ZnO (102)**	**ZnO (110)**	**HAp(200)**	**HAp(203)**
5h	32.20°	34.85°	36.67°	47.95°	56.99°	-	-

1D	32.20º	34.84º	36.68º	48.00º	56.98º	-	-
3D	31.62º	34.27º	36.08º	47.42º	56.51º	-	-
3D ref	32.17º	34.77º	36.63º	47.92º	56.96º	-	-
1W	32.27º	34.90º	36.47º	48.00º	57.09º	-	-
1W ref	32.25º	34.85º	36.71º	47.98º	57.00º	-	-
2W	31.96º	34.58º	36.39º	47.69º	56.75º	-	-
2W ref	32.25º	34.85º	36.61º	48.00º	57.00º	-	-
1M ref	32.28º	34.93º	36.72º	48.03º	57.04º	-	-
2M	31.85º	34.55º	36.36º	47.68º	56,66º	21.76º	45.3º

Table 9: XRD peaks position of ZnO samples soaked in SBF

The crystal structure remains exactly the same during the first month. All the XRD peaks were indexed and well matched with the standard hexagonal structure of ZnO. In some cases, a diffraction contribution always positioned at 33º appeared and was due to diffraction coming from the silicon (Si) substrate. No other characteristic peaks related to impurities and any intermediate materials were observed, which further confirms that the diffractograms reflects a pure ZnO structure [42].

Finally, for the sample soaked in SBF for 2 months, there is an appreciation of 2 additional XRD peaks, one at 21,76º, and one at 45,3º, corresponding to (200) and (203) planes of HAp crystal structure.

This conclusion was reached by comparing the typical pattern of HAp (*Figure 34*) with the pattern of sample 2M. It is evident that all of them are related to the beginning of precipitation of HAp on the surface of the sample.

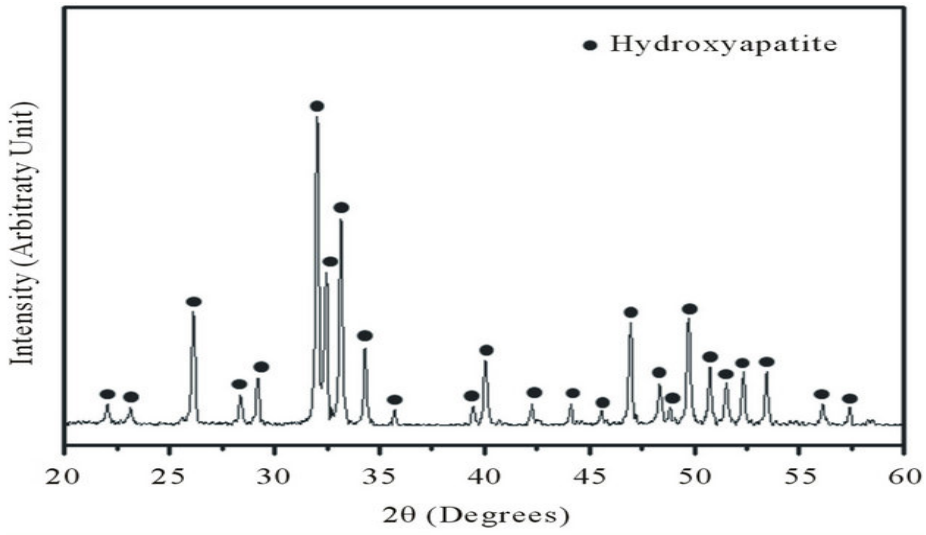

Figure 34: Typical pattern of HAp

4.1.5 Inductively Coupled Plasma (ICP) mass spectrometry

In order to study the biodegradation of porous ZnO when soaked in the media mentioned, ICP analyses have been performed on the solutions after removing the samples to evaluate the concentration of Ca^{2+}, PO^{4--} and Zn^{2+} ions versus the soaking time. The aim of this analysis is twofold: (1) to evaluate the precipitation of P and Ca from the SBF solution to the ZnO sample, and (2) to get information about the kinetics of degradation, by evaluating the amount of Zn^{2+} ions released from the sample to the SBF solution.

Since the EDS maps and the atomic composition of the samples obtained for the samples showed an increase of P and Ca amounts versus the soaking time, ICP analyses of the corresponding SBF solution were expected to show a decrease of these elements. The P decreases to zero mainly after the first month soaking time, while Ca slightly increases and decreases until finally reducing its amount during the second month.

This fact is due to the bioactivity of the sample when soaking it in the SBF solution: the sample surface acts as nucleation sites for the HAp precipitation, thus recruiting Ca and P from the SBF.

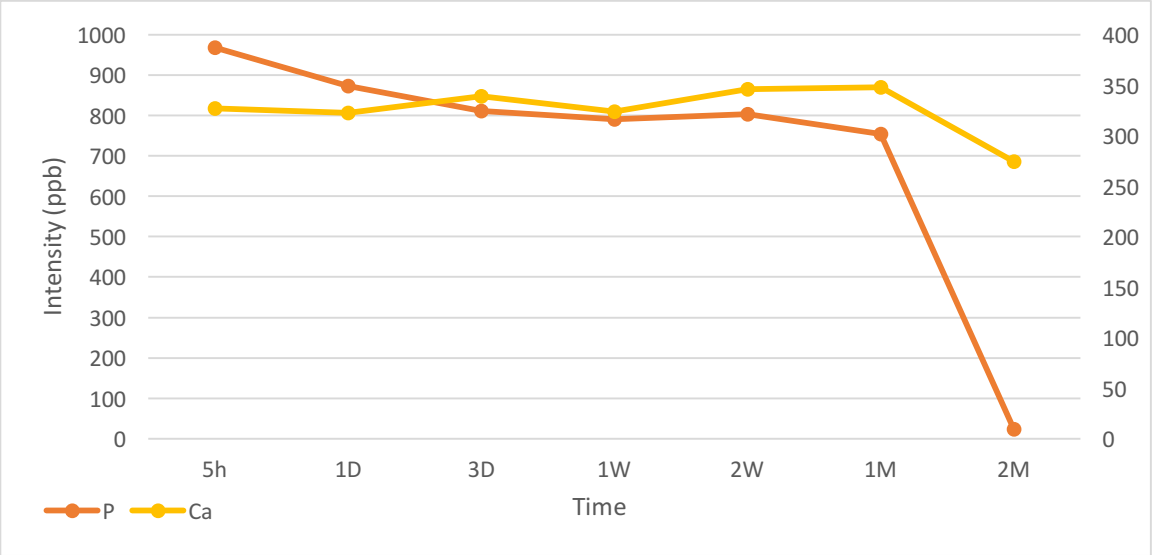

Figure 35: ICP results when evaluating the evolution of Ca and P of the SBF solution among the time

On the other hand, Zn^{2+} concentration increases due to the biodegradation of the samples.

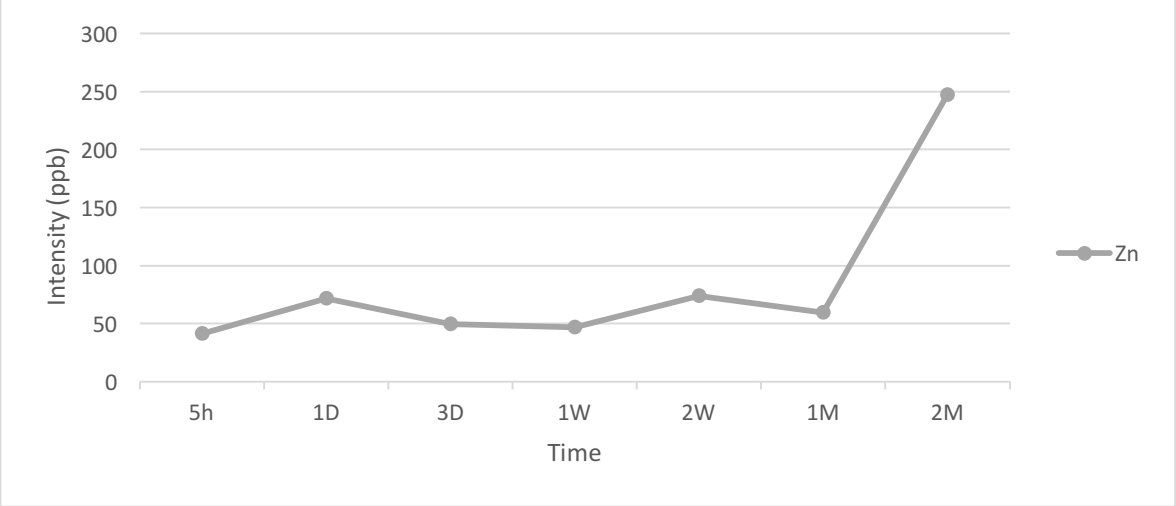

Figure 36: ICP results when evaluating the evolution of Zn of the SBF solution among the time

4.2 *In-vitro* evaluation of bioactivity and biodegradation properties of porous ZnO/GO structures soaked in SBF solution

Hypothesizing that a GO coating could improve the formation of apatite layer, the same physico-chemical studies were carried out on 6 porous ZnO samples coated with GO.

4.2.1 Attenuated Total Reflection (ATR)

Concerning ATR analyses, the results are very similar to the ones obtained by soaking the porous ZnO samples into SBF solution (reported at 4.1.1).

The different phosphates bands can be observed, one positioned between 960 and 1190 cm^{-1} corresponding to v_3 mode, a second one at 940 cm^{-1} corresponding to v_1 mode and another between 540 and 660 cm^{-1} corresponding to v_4 mode. The presence of OH groups is also noticed between these two bands. The amide I band is also present with the corresponding band, located in the range 1600 – 1700 cm^{-1} and with a maximum at 1640 cm^{-1}.

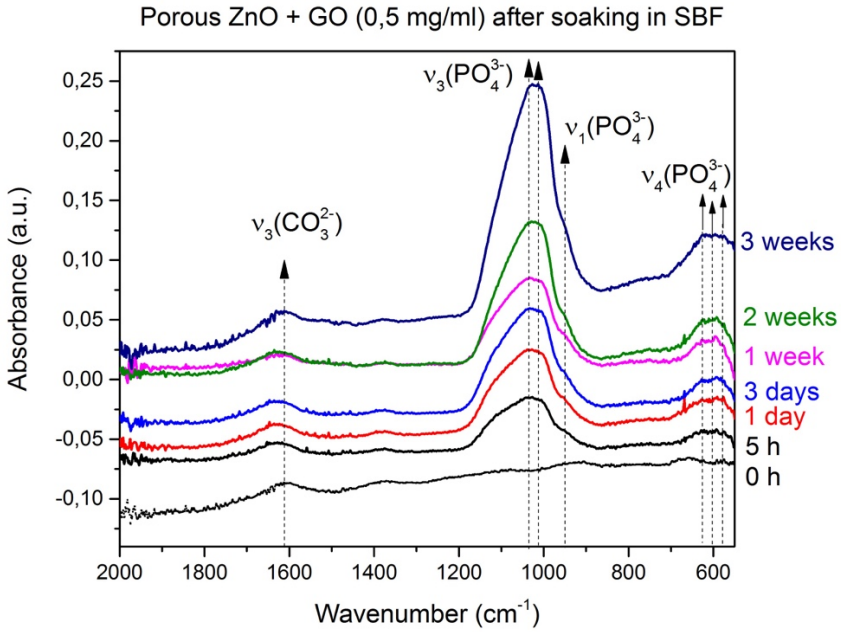

Figure 37: ATR spectra of ZnO/GO samples soaked in SB

4.2.2 Energy-Dispersive X-Ray Spectroscopy (EDS)

Regarding the chemical composition studied with EDS maps, also in this case an increase of Ca and P amounts is obtained while increasing the soaking time.

By comparing those results with the ones obtained with porous ZnO samples soaked in SBF, it can be observed that the precipitation of Ca and P onto the ZnO/GO surface is more quick. Moreover, the corresponding amount obtained for the same soaking time is higher when the sample is coated with GO, due to the more pronounced bioactivity behaviour.

As it was mentioned in Paragraph 4.1.2, those analyses cannot affirm that there is forming hydroxyapatite as, for its formation, a Ca/P stoichiometry ratio equal to 1.67 is required.

In *Figure 38* it is shown the evolution of Ca (purple) and P (yellow) amounts versus time, showing the increase of the Ca/P stoichiometry, reaching a value of 0.7 after soaking for 3W. In *Figure 39 the* evolution of the EDS maps along the time.

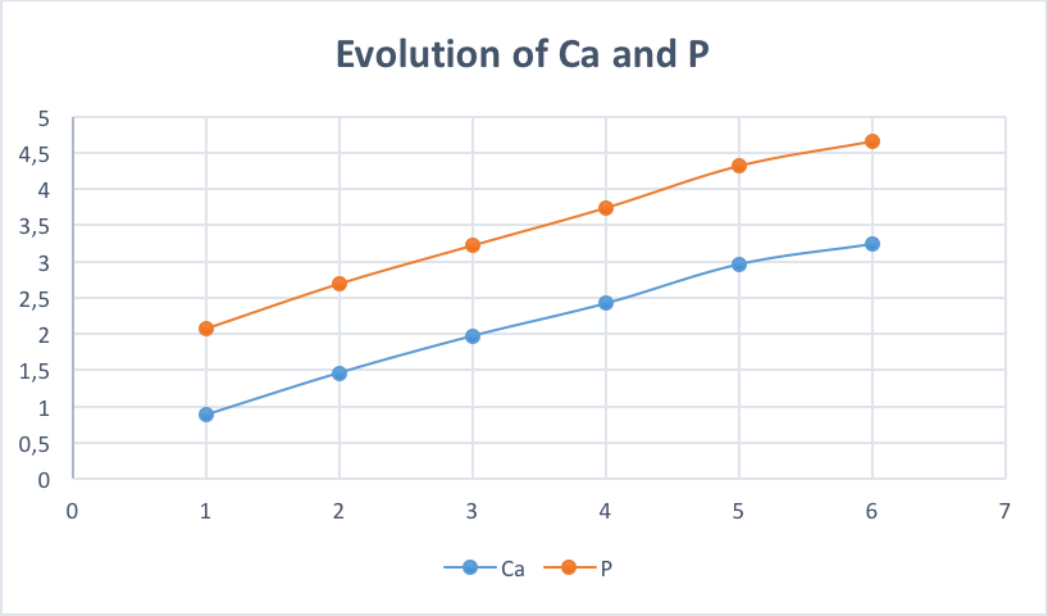

Figure 38: Evolution of Ca and P versus the soaking time

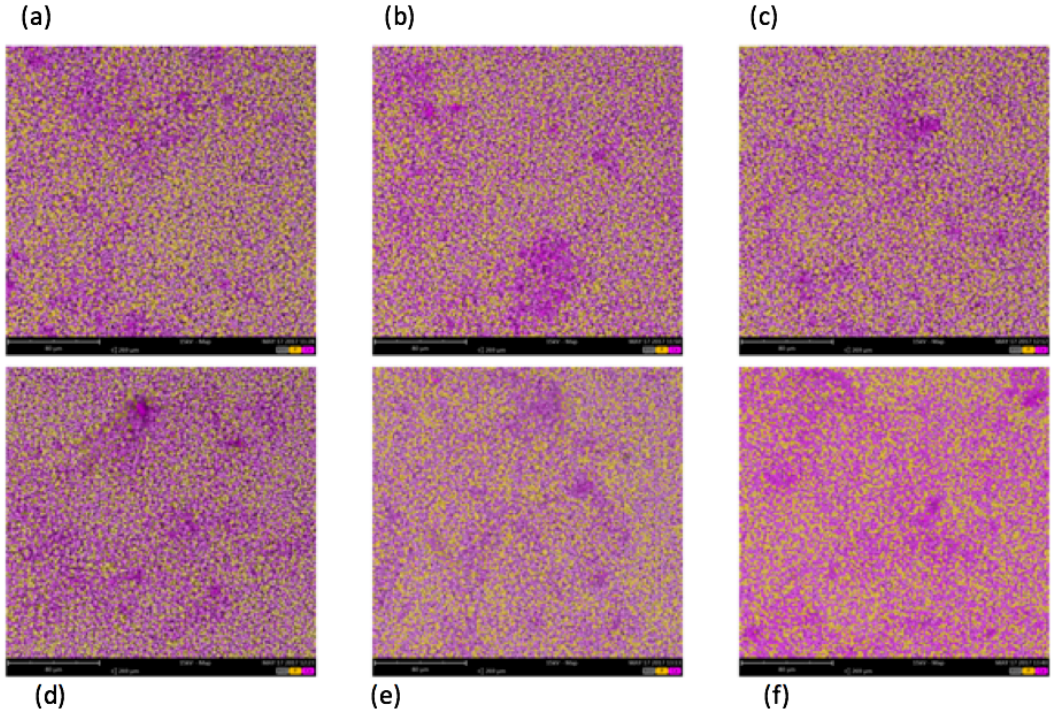

Figure 39: EDS map of the ZnO samples coated with GO and soaked in SBF for: (a) 5h, (b) 1D, (c) 3D, (d) 1W, (e) 2W, (f) 3W

4.2.3 Field-Emission Scanning Electron Microscopy (FESEM)

Images about the evolution of the surface morphology of the samples were obtained using FESEM characterization. In order to obtain biological results, the morphology of ZnO coated with GO was studied in three different concentrations: 0.1 mg / ml, 0.5 mg / ml and 1 mg / ml. With all the data obtained it was decided to use the concentration of 0.5mg / ml to proceed with the experiments, corresponding to the optimal coating from our point of view, therefore by coating ZnO with GO at this concentration it is expected that the bioactivity for tissue engineering would be promoted.

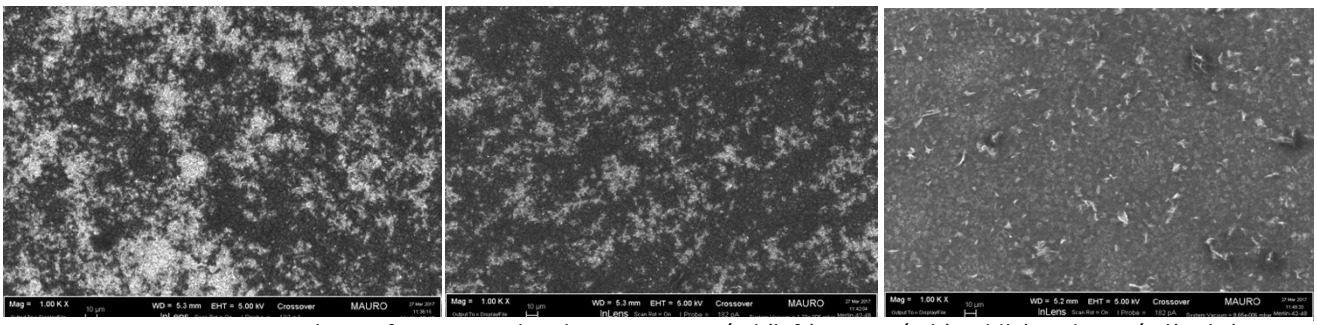

Figure 40: FESEM analyses of ZnO coated with GO at 0.1mg/ml (left), 0.5mg/ml (middle) and 1mg/ml(right)

The formation of calcium phosphates on the surface of the sample is easy to be identified in the following images. The sample soaked for only 5h shows formations of less than 200nm of diameter while, as the soaking time increases, the amount of calcium phosphates increases too. Finally, in *Figure 46* it is reported a compact structure at a magnitude of 350,00KX.

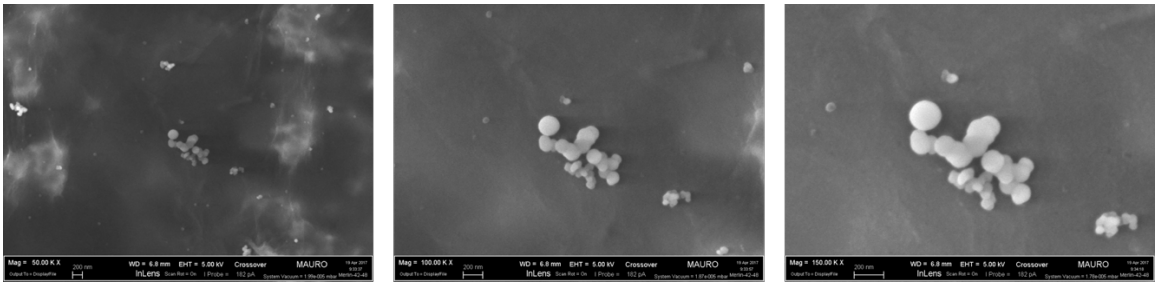

Figure 41: FESEM GO with SBF 5h. 50,00 KX left, 100,00 KX middle and 150,00 KX right

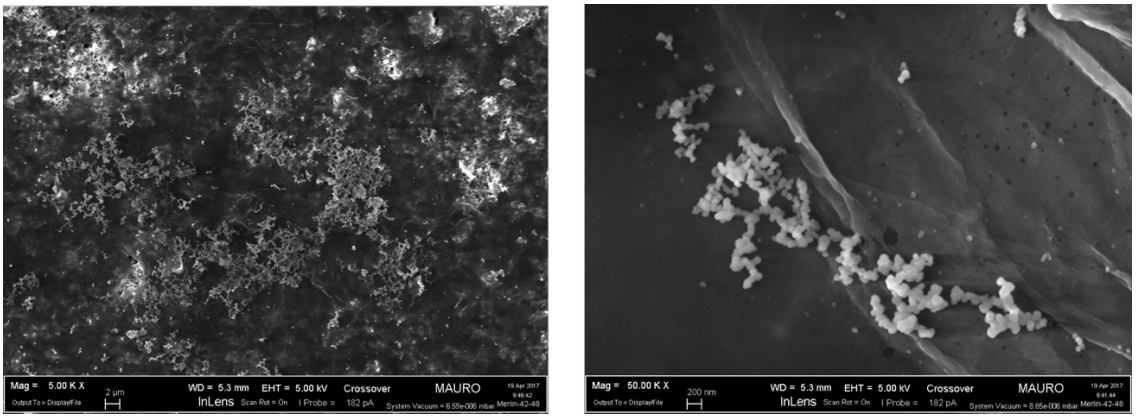

Figure 42: FESEM GO with SBF 1D. 5,00 KX left, 50,00 KX right

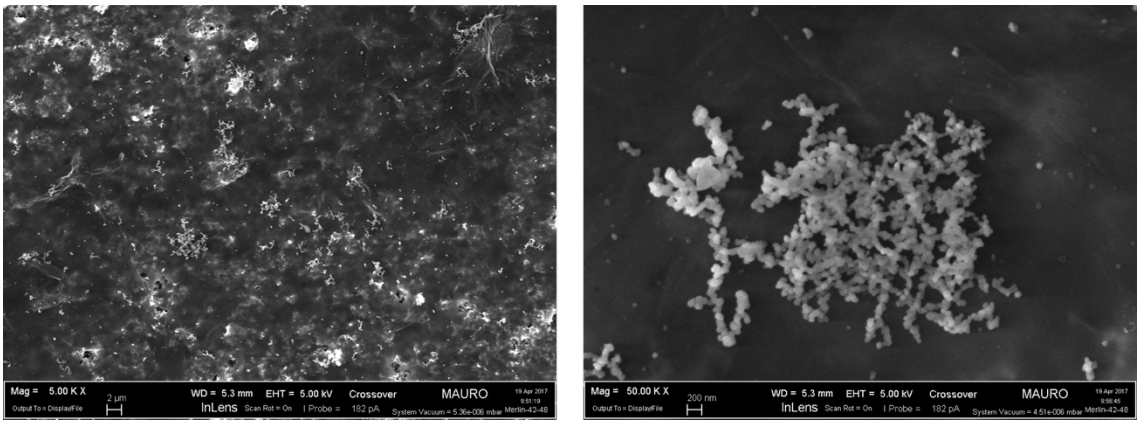

Figure 43: FESEM GO with SBF 3D. 5,00 KX left, 50,00 KX right

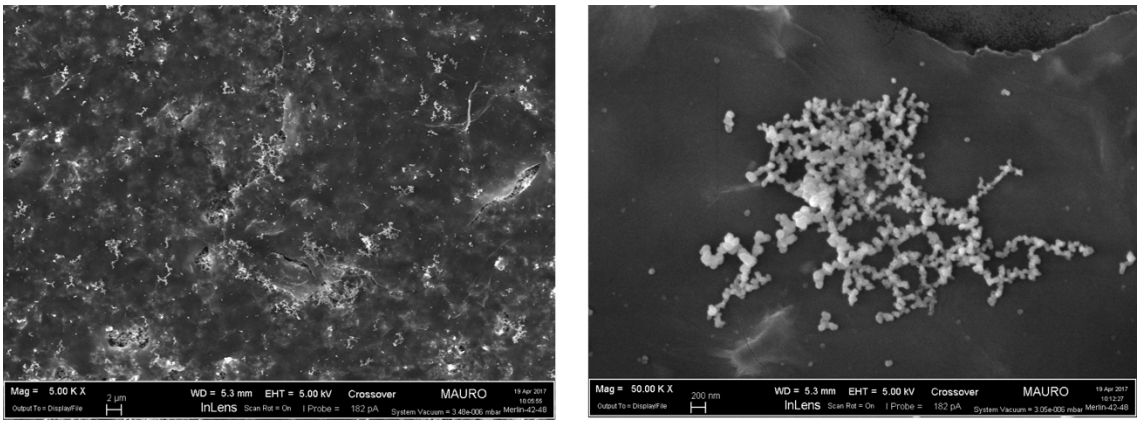

Figure 44: FESEM GO with SBF 1W. 5,00 KX left, 50,00 KX right

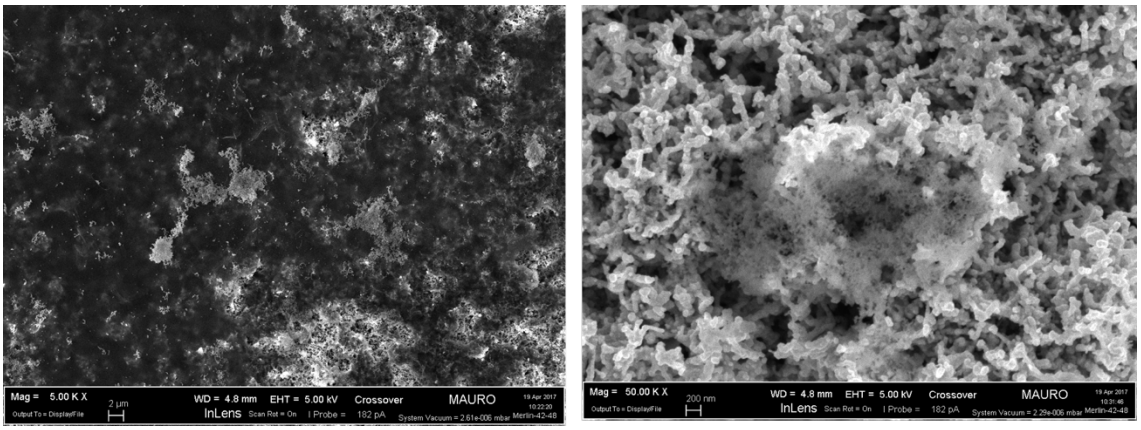

Figure 45: FESEM GO with SBF 2W. 5,00 KX left, 50,00 KX right

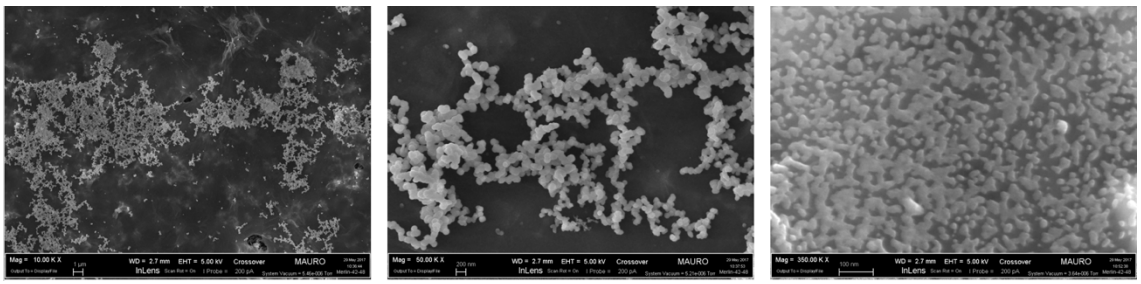

Figure 46: FESEM GO with SBF 3W. 10,00KX left, 50,00KX middle, 350,00KX right

This refers to the ZnO/GO sample soaked in SBF for 3 weeks, showing that the precipitation of a compact HAp layer on the ZnO/GO surface started to occur, as also witnessed by the XRD results below.

4.2.4 X-Ray Diffraction (XRD)

Figure 47 show the XRD patterns of all the investigated ZnO/GO samples, after soaking in SBF up to 3W. All the detected peaks, together with the corresponding 2θ positions and Miller indices are listed in *Table 10*. The obtained results are similar to those obtained for the porous ZnO samples soaked in SBF without the presence of GO. However, by adding a GO coating on the samples, the precipitation of HAp is more quick. This conclusion has been reached by comparing the XRD patterns of the ZnO/GO sample soaked in SBF for 3W and of the ZnO sample soaked for 1M. While the XRD pattern of the ZnO sample soaked for 1M only shows the diffraction peaks characteristic of wurtzite ZnO, in the 3W ZnO/GO sample there is an appreciation of an HAp peak, positioned at 45.46º and ascribed to the reflection of (203) planes.

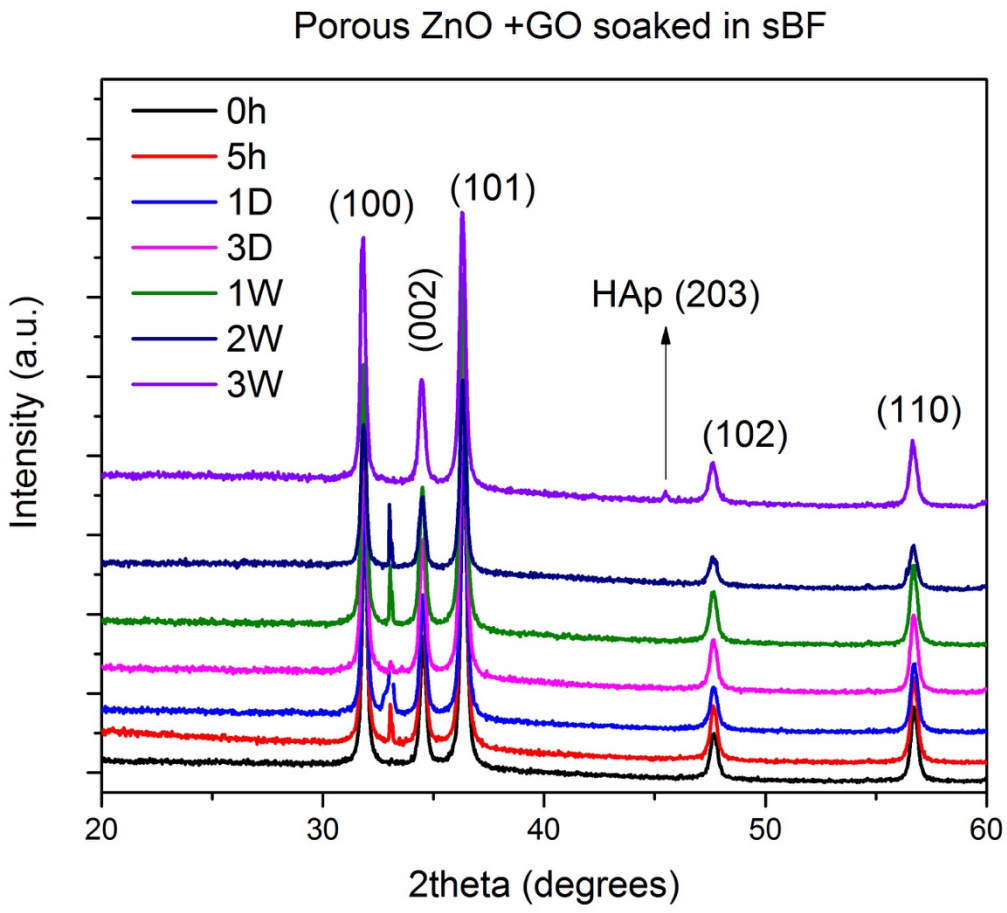

Figure 47: XRD pattern of porous ZnO samples coated with GO and soaked in SBF

	2θ position					
Sample	**ZnO (100)**	**ZnO (002)**	**ZnO (101)**	**ZnO (102)**	**ZnO (110)**	**HAp**
5h	31.88º	34.54º	36.37º	47.69º	56.73º	
1D	31.88º	34.54º	36.37º	47.67º	56.78º	
3D	31.86º	34.48º	36.35º	47.67º	56.73º	
1W	31.86º	34.48º	36.32º	47.72º	56.75º	
2W	31.83º	34.48º	36.32º	47.67º	56.73º	
3W	31.80º	34.48º	36.32º	47.62º	56.65º	45.46º

Table 10: XRD peaks position of ZnO/GO samples soaked in SBF

4.2.5 Inductively Coupled Plasma (ICP) mass spectrometry

To study the biodegradation of ZnO samples coated with GO when immersed in SBF, the ICP analysis of the SBF solution after removing the sample was performed.

Taking into account that the EDS maps and the atomic composition of the samples show an increase of P and Ca among the time, ICP analyses of the SBF solution were expected to show a decrease of this elements.

Both of the elements showed a similar behaviour. During the first hours their concentrations decrease, assuming that they precipitate on the sample surface, but when reaching the first week of soaking time, their concentration increases again, with a final decrease during the second week, corresponding to the beginning of HAp precipitation.

The evolution of P intensity changes much more that the one corresponding Ca.

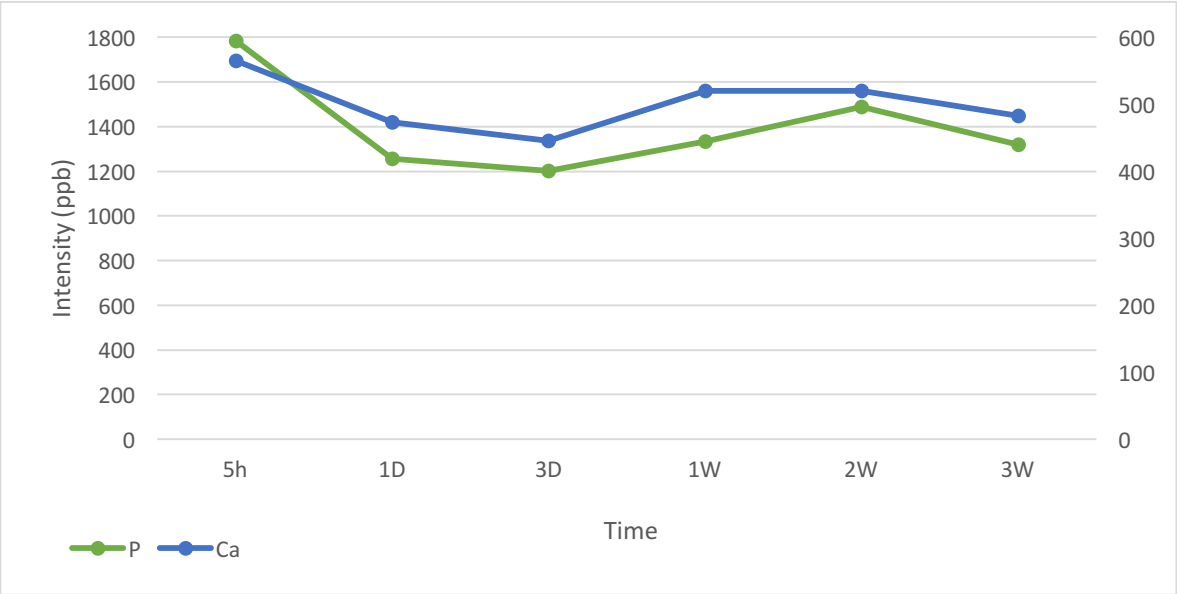

Figure 48: ICP results when evaluating the evolution of Ca and P of the SBF solution among the time

The evolution of Zn^{2+} ions versus time is strongly different from what observed for the samples without the GO coating; it slightly increases, especially after soaking the sample for 1W. Therefore, the presence of the GO coating helps in limiting the degradation of the underlying porous ZnO layer.

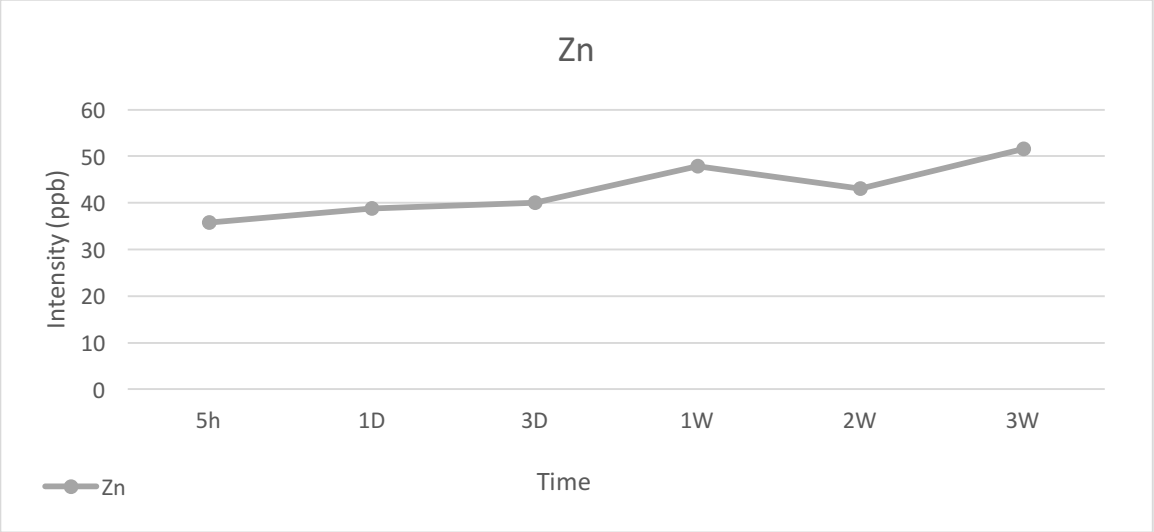

Figure 49: ICP results when evaluating the evolution of Zn of the SBF solution among the time

By comparing those results with the ZnO samples, and as it is demonstrated with the other characterization results, both, biodegradation and bioactivity, are noticed earlier when coating the sample with GO.

4.3 *In-vitro* evaluation of bioactivity and biodegradation properties of porous ZnO structures soaked in eMEM

4.3.1 Attenuated Total Reflection (ATR)

The samples soaked in eMEM show different ATR spectra. They are also characterized by the phosphates bands, however by soaking the sample into this medium, peaks in the region between 1400 and 1600 cm^{-1} were obtained, due to carbonate ions. These carbonate bands are assigned to surface carbonate ions, rather than carbonate ions in the lattice of phosphate ions. The amide I band (1600 – 1700 cm^{-1}) is also present.

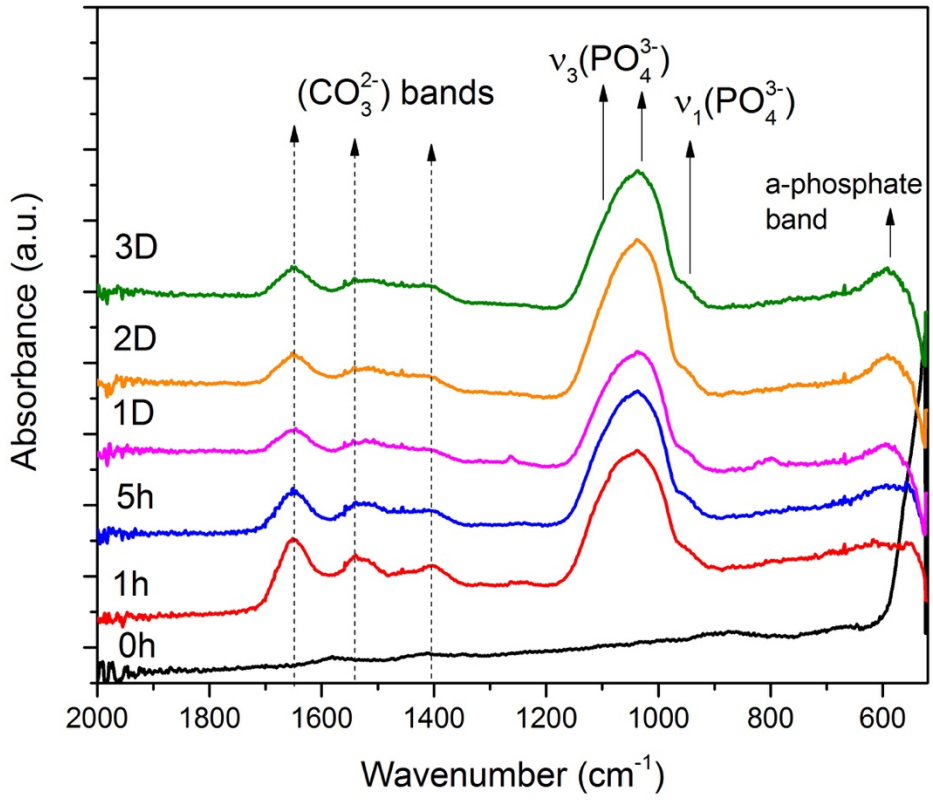

Figure 50: ATR spectra of ZnO samples soaked in eMEM

4.3.2 Field-Emission Scanning Electron Microscopy (FESEM)

The following images show the evolution of this zinc phosphates formations among the time. First, after 5h, then after 1D, 2D and finally 3D, which is the typical time needed to well appreciate such structures formation.

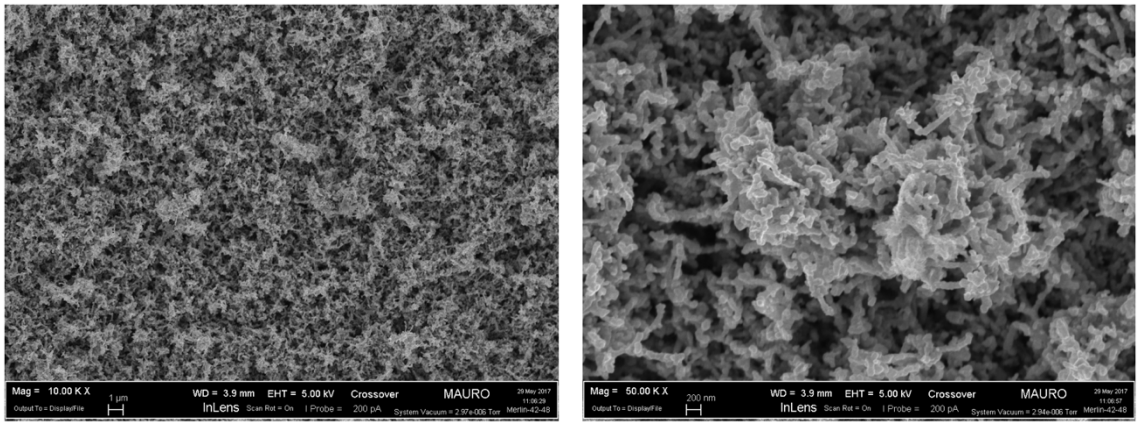

Figure 51: FESEM image of ZnO soaked in eMEM for 5h. 10,00KX left, 50,00KX right

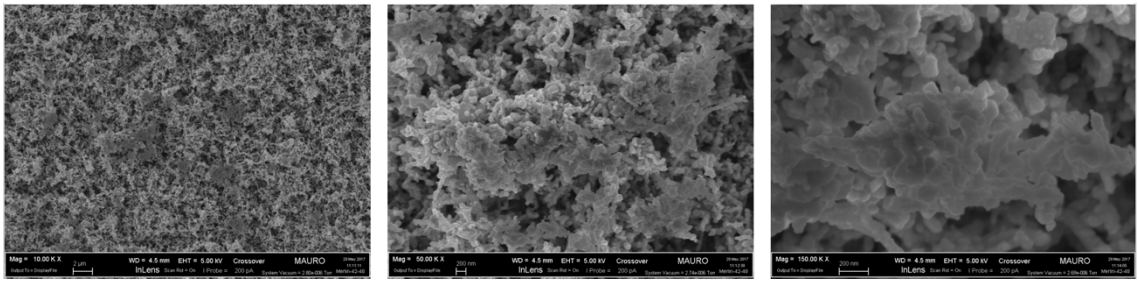

Figure 52: FESEM image of ZnO soaked in eMEM for 1D. 10,00KX left, 50,00KX middle, 150,00KX right

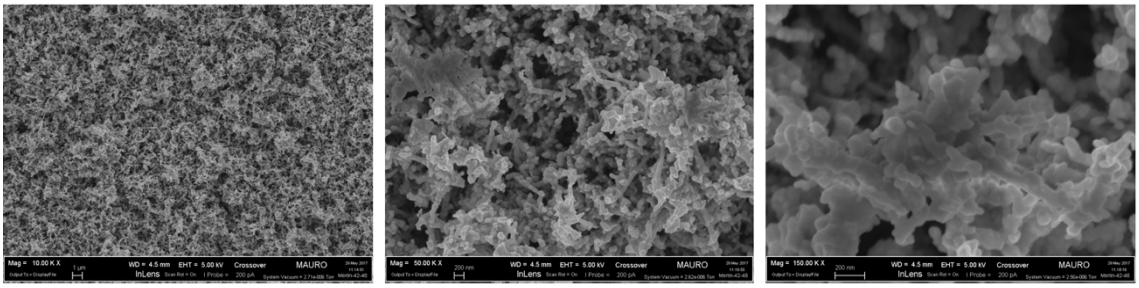

Figure 53: FESEM image of ZnO soaked in eMEM for 2D. 10,00KX left, 50,00KX middle, 150,00KX right

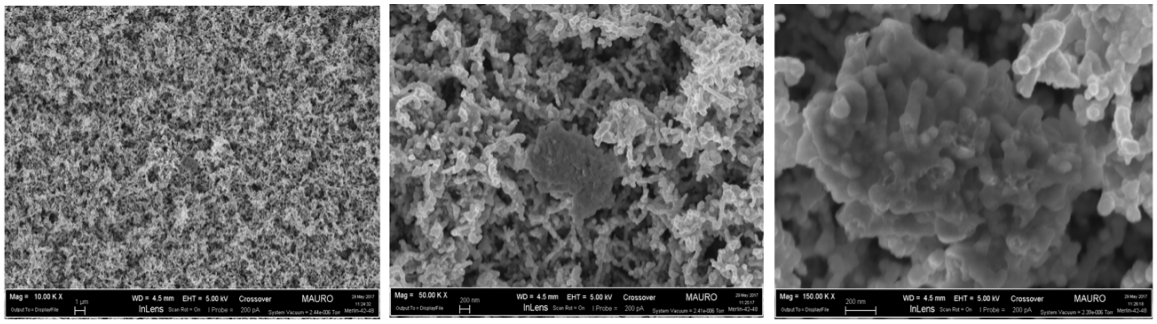

Figure 54: FESEM image of ZnO soaked in eMEM for 3D. 10,00KX left, 50,00KX middle, 150,00KX right

Concerning the samples soaked in eMEM, by increasing the soaking time in medium for cell culture there is an appreciation of the growth of zinc phosphates formations. This can be due to the lower solubility product constant of $Zn_3(PO_4)_2$ than that of $Ca_3(PO_4)_2$. Therefore, in aqueous solution PO_4^{3-} ions combine more easily with Zn^{2+} ions than with Ca^{2+}. This conclusion was reached by comparing these samples with those soaked in SBF, and knowing that in the medium for cell culture there is no formation of calcium phosphates.

By taking a look to the ATR-IR spectrum shown in *Figure 21*, *Figure 22* and *Figure 50*, it is easy to see that the phosphates band is similar when soaking in any of both solutions (eMEM and SBF). According to this fact and, since there is no possibility of calcium phosphates formation, it is believed that the observed structures are due to the formation of zinc phosphates.

Figure 55 compares two representative FESEM images of the structures obtained by soaking the samples either in SBF or eMEM media. The first one is ascribed to calcium phosphates whereas the second is ascribed to zinc phosphates, which looks like more amorphous and compact than calcium phosphates structures.

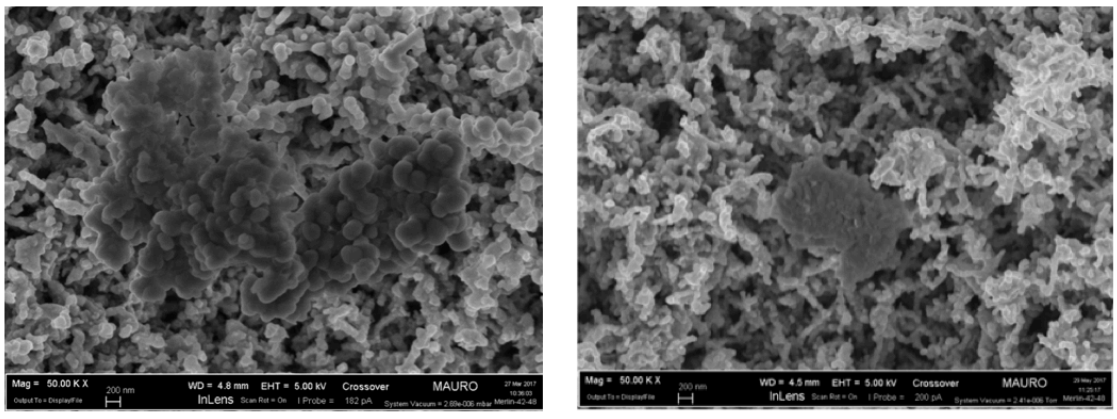

Figure 55: FESEM image of ZnO soaked with eMEM (left) and ZnO soaked with SBF (right)

4.3.3 X-Ray Diffraction (XRD)

Concerning the samples soaked with eMEM, XRD analyses have been performed onto 5 porous ZnO samples. The one corresponding to the 1h soaking time is missing since it was damaged during ATR-IR analysis.

Figure 56 report the results obtained for the 5h, 1D, 2D and 3D soaking time samples.

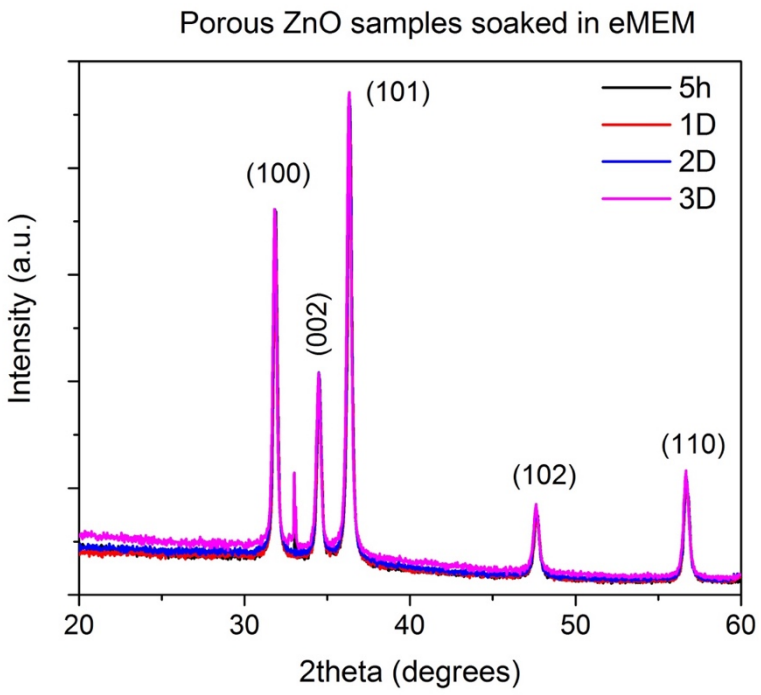

Figure 56: XRD pattern of porous ZnO samples soaked in eMEM

	2θ position					
Sample	**ZnO (100)**	**ZnO (002)**	**ZnO (101)**	**ZnO (102)**	**ZnO (110)**	**Si**
5h	31.88°	34.50°	36.35°	47.70°	56.73°	33.12°
1D	31.88°	34.54°	36.35°	47.67°	56.70°	-
2D	31.83°	34.48°	36.35°	47.61°	56.65°	-
3D	31.80°	34.46°	36.32°	47.61°	56.67°	33.00°

Table 11: XRD peaks position of ZnO samples soaked in eMEM

The results show that the crystal structure remains the same. Also, in these analyses no HAp-related peak was expected since no calcium phosphates could be formed in eMEM.

4.3.4 Inductively Coupled Plasma (ICP) mass spectrometry

When soaking porous ZnO samples in eMEM, it is found that the evolution of P and Ca concentrations is very unstable. At a first point it slightly increases, then decreases along the first day, and finally increases again along the last two days, approaching values similar to the starting ones. This final increase can be possibly linked to the dissolution of Zn in the following figure: since the surface dissolves, it can release not only Zn^{2+} cations, but also ZnO and $Zn(PO_4)_2$ structures, and what is detected by ICP is an overall increase of Zn and P in the solution. While Ca evolution is really small (between 350 and 400 ppb), P evolution is bigger.

On the other hand, the evolution of Zn^{2+} versus time shows an important increase, due to the biodegradation of the sample, when soaking it in eMEM.

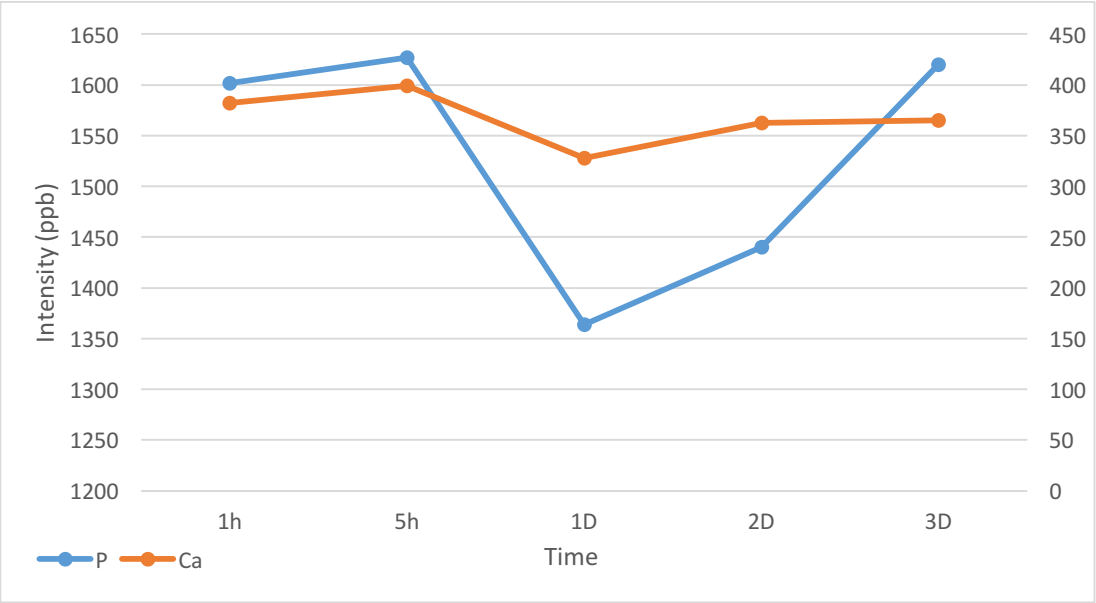

Figure 57: ICP results when evaluating the evolution of Ca and P of the medium for cells culture among the time

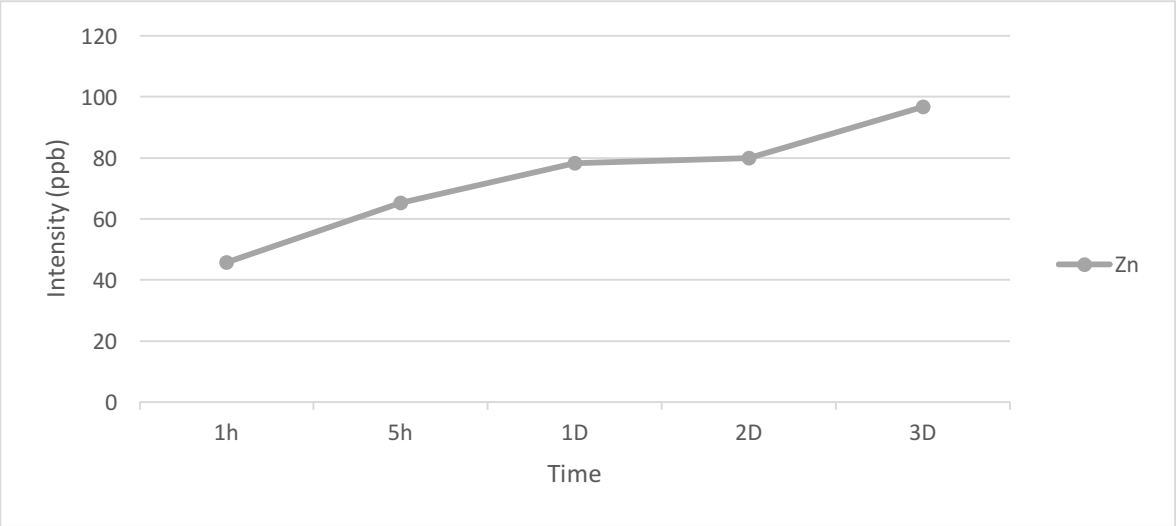

Figure 58: ICP results when evaluating the evolution of Zn of the medium for cells culture among the time

4.4 Uptaking/releasing Rhodamine-β dye molecule on porous ZnO structures for drug delivery applications

As introduced in Paragraph 3.4, Rhodamine-B dye was used in this thesis work as a model for studying the capacity of the porous ZnO thin films to uptake and release molecules for future drug delivery applications.

The experiments were done using two porous ZnO samples. The uptake experiment was performed on both and then, one was used for the release experiment and the other for obtaining the fluorescence images.

For the uptake experiment, the characteristic absorption peak at the specific wavelength of 552 nm was monitored. Therefore, if Rhodamine-B was loaded on the porous ZnO sample, the intensity of the characteristic peak was expected to decrease, since the intensity depends on the amount of Rhodamine still present in the solution surrounding the ZnO sample. So, to evaluate the loading of Rhodamine against time, the decrease of the absorption intensity at 552 nm against time by analysing the UV spectrum of different Rhodamine solutions was performed.

After leaving the sample into a flask covered with aluminium paper stirring at 600rpm for 24h at room temperature, and collecting different aliquots of Rhodamine solution after 1h, 2h, 3h, 4h 5h and 24h, the results shown in *Figure 59* were obtained.

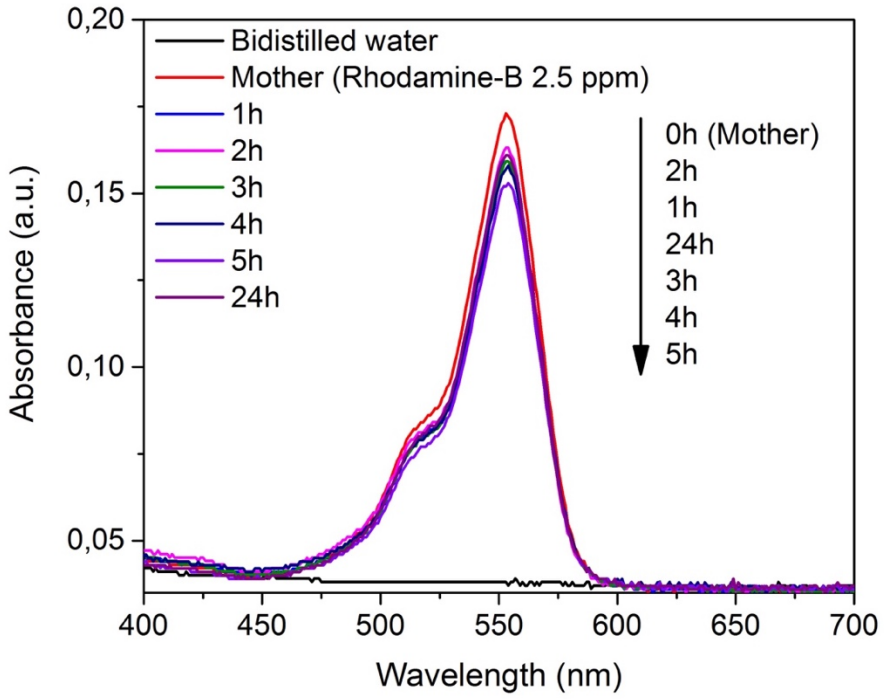

Figure 59: Absorption spectrum of Rhodamine-B in the presence of porous ZnO thin films at different time interval

All the absorbance values corresponding to 552 nm characteristic peak are tabulated in *Table 12.*

The starting solution (SS) is also tabulated in order to evaluate the percentage of Rhodamine loaded on the porous ZnO sample versus time.

Sample	**SS**	**1h**	**2h**	**3h**	**4h**	**5h**	**24h**
552 nm	0.173	0.161	0.163	0.159	0.158	0.153	0.161

Table 12: Amount of Rhodamine-B at 552 nm

It was expected to be reduced among the time, following the 1h-2h-3h-4h-5h-24h order, as the sample was supposed to uptake more and more Rhodamine-B each hour. The fact that 2h and 24h values are in those position indicates that the problem of the base line is clearly present. However, for the 24h value, it could be also possible that after the prolonged time of soaking the sample in the Rhodamine solutions for 24h, part of the Rhodamine previously loaded on the sample surface has been desorbed, coming back to the solution, and inducing the increase of the absorption peak after 24h.

The calibration curve obtained with Rod 2.5ppm diluted in water was normalized and the results is shown in Figure 60. The linearization of those results is plotted in red and was used for obtaining the concentration of Rhodamine at each period of time.

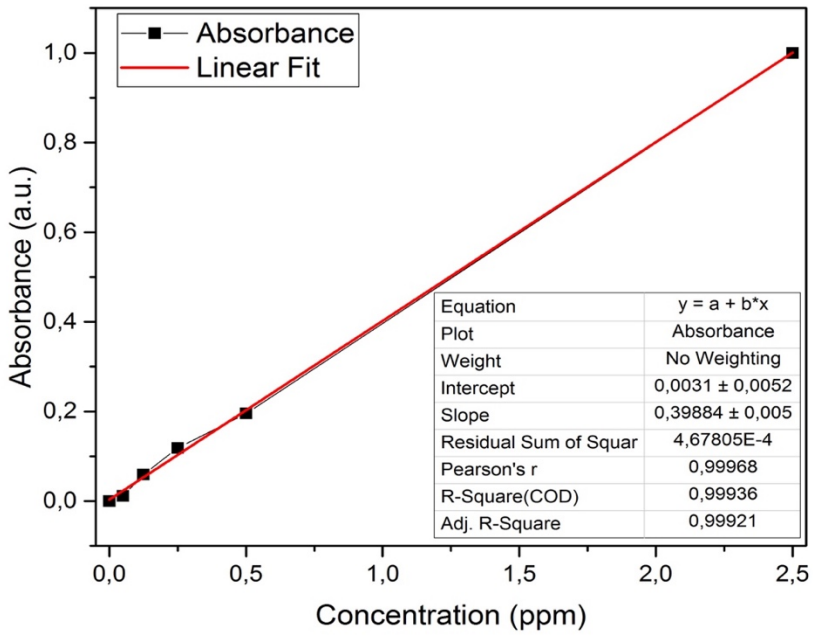

Figure 60: Calibration curve of Rhodamine 2.5 ppm diluted in H_2O normalized

By combining the absorbance values at 552 nm wavelength found in *Table 12* with the linear fit of the calibration curves normalized, it is possible to quantiavely estimate the amount of Rhodamine uptaken.

In Figure 61 there are shown, on one hand, the concentration of Rhodamine in solution and, on the other hand, the percentage of Rhodamine that the sample have uptake. Those values are opposite due to the fact that with this experiment the results obtained are from the solution but the uptake values are the difference between the maximum (2.5 ppm) and the concentration ate the different time points.

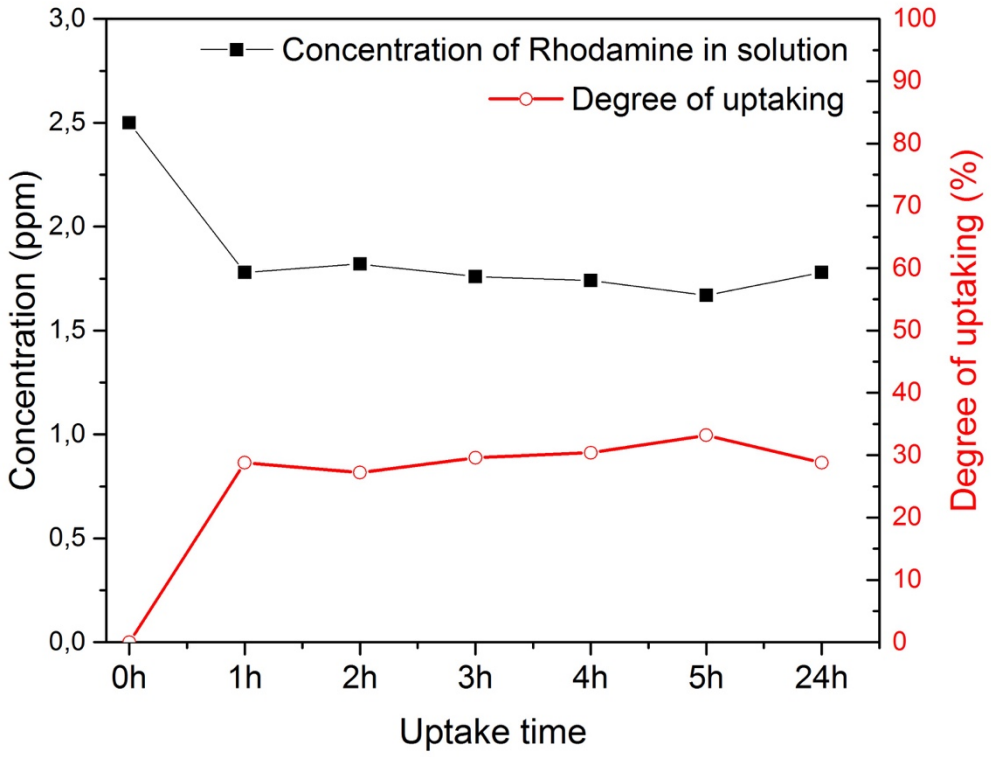

Figure 61: Concentration of Rhodamine in solution and degree of uptaking

Knowing that for the starting solution of Rhodamine with concentration of 2,5 ppm, the amount of Rhodamine is 5,6 µmol, the amount of Rhodamine uptaken from porous ZnO thin film by means of percentage and µmol is reported in *Table 13.*

Sample	SS	1h	2h	3h	4h	5h	24h
%	0	28,8	27,2	29,6	30,4	33,2	28,8
μmol	0	1,61	1,52	1,66	1,7	1,86	1,61

Table 13: Amount of Rhodamine uptaken from porous ZnO thin film by means of percentage (%) and μmol

Concerning the release experiment, after leaving the sample (previously used for the uptake experiment) into a brownish plastic tube filled with 20 ml of SBF solution and a magnetic stirrer, stirring at 150 rpm with a constant temperature of 37ºC, 100μl of the solution were extracted at each selected time point in order to analyse the UV spectrum of the different SBF solution samples.

While Rhodamine was released from the sample to the solution, the characteristic peak at the specific wavelength of 552 nm was expected. If Rhodamine-B would have been released from the sample to the solution, the intensity of the characteristic would be expected to increase, since the intensity depends on the amount of Rhodamine present in the solution surrounding the ZnO sample. The higher the absorption of this peak, the higher the amount of released Rhodamine from the sample.

The results are shown in *Figure 62.*

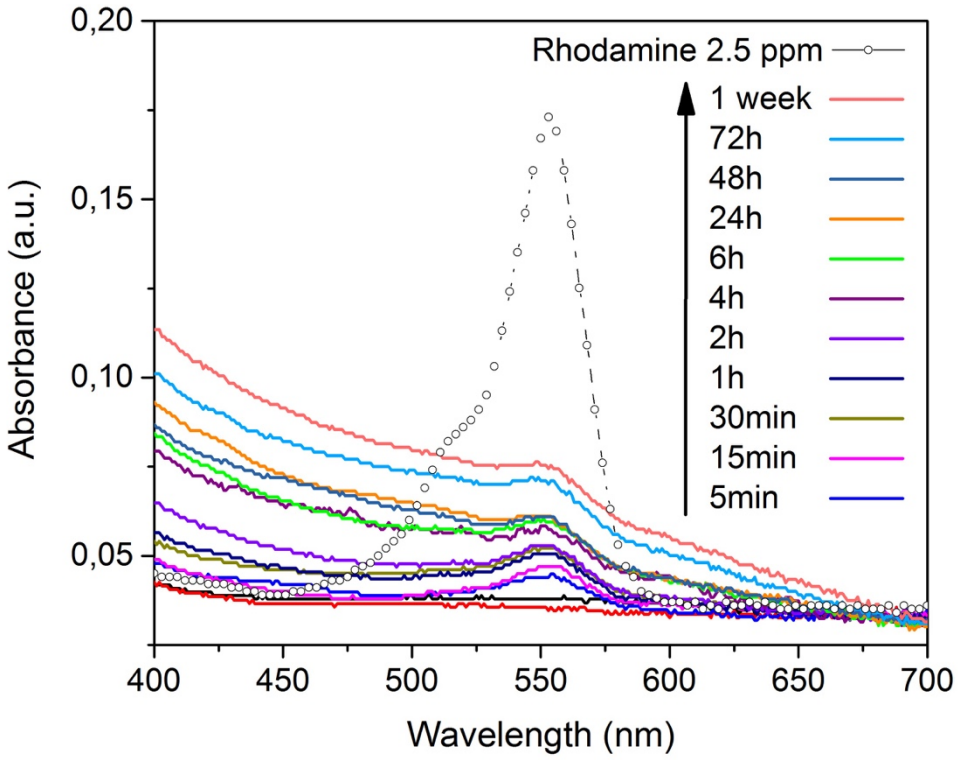

Figure 62: Release spectrum of Rhodamine-B in presence of porous ZnO thin films at different time intervals

Those results show a slight peak at 552 nm wavelength position related to Rhodamine-B release. This peak begins to be noticed after only leaving the sample for 5 min and increases among the time.

All the absorbance values corresponding to 552 nm characteristic peak are tabulated in *Table 14*.

Sample	**SS**	**5min**	**15min**	**30min**	**1h**	**2h**	**4h**	**6h**	**24h**	**48h**	**72h**	**1week**
552 nm	0.173	0.045	0.047	0.053	0.051	0.053	0.057	0.059	0.061	0.061	0.071	0.075

Table 14: Amount of Rhodamine-B at 552 nm

The results of the calibration curve obtained with SBF diluted in water normalized are shown in Figure 63. The linearization of those results is plotted in red and used for obtaining the concentration of Rhodamine at each period of time.

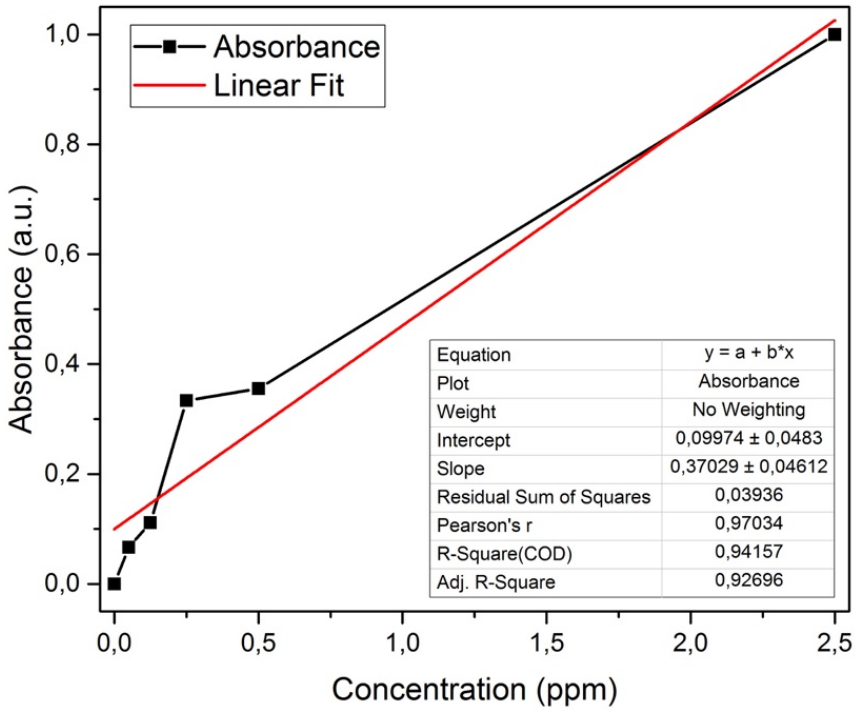

Figure 63: Calibration curve of SBF diluted in H_2O normalized

Again, by combining the absorbance values at 552 nm wavelength found in Table 14 with the linear fit of the calibration curve normalized, it is possible to quantiavely estimate the amount of Rhodamine released.

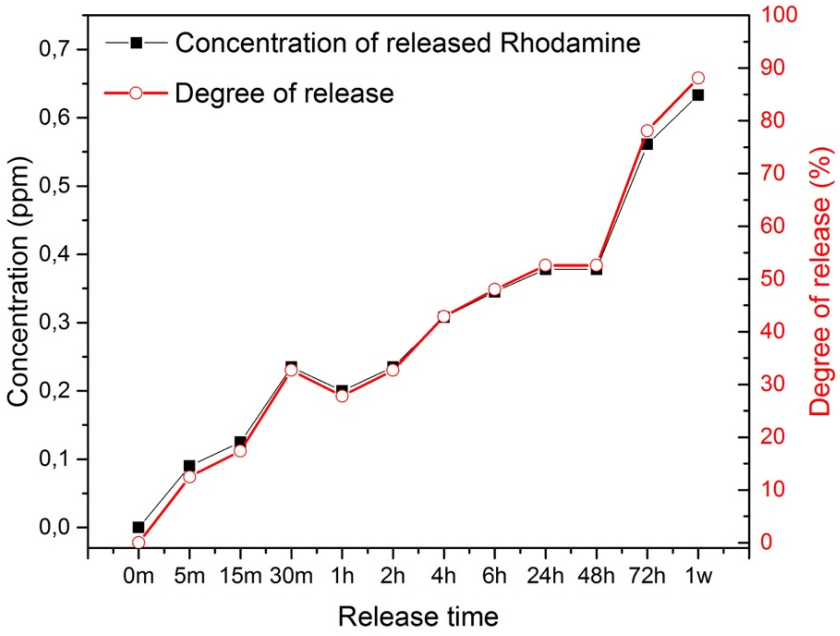

Figure 64: Concentration of released Rhodamine and degree of release

In Figure 64 there are shown, on one hand, the concentration of released Rhodamine and, on the other hand, the degree of Rhodamine released.

For the starting solution of Rhodamine released in SBF, the amount of Rhodamine is 1,61 µmol, which is equal to the value of Rhodamine uptaken after 24h, that is the effective amount of Rhodamine loaded on the ZnO sample. The amount of Rhodamine released from the porous ZnO thin films by means of percentage and µmol are tabulated in *Table 15*.

Sample	SS	5min	15min	30min	1h	2h	4h	6h	24h	48h	72h	1week
%	0	12,5	17,4	32,7	27,8	32,7	42,9	48	52,6	52,6	78,1	88,1
µmol	0	0,20	0,28	0,53	0,45	0,53	0,69	0,77	0,85	0,85	1,26	1,42

Table 15: Amount of Rhodamine released from porous ZnO thin film by means of percentage (%) and µmol

Rhodamine dyes fluoresce and can thus be detected with instruments called a fluorescence microscope. In this thesis, for observing the capacity of porous ZnO thin films in uptaking Rhodamine-B, fluorescence images of the sample previously used for the uptaking experiment have been obtained by a Nikon Eclipse T*i* fluorescence microscope.

Figure 65 show the images taken when observing the red channel at 4x, 20x and 40x, respectively.

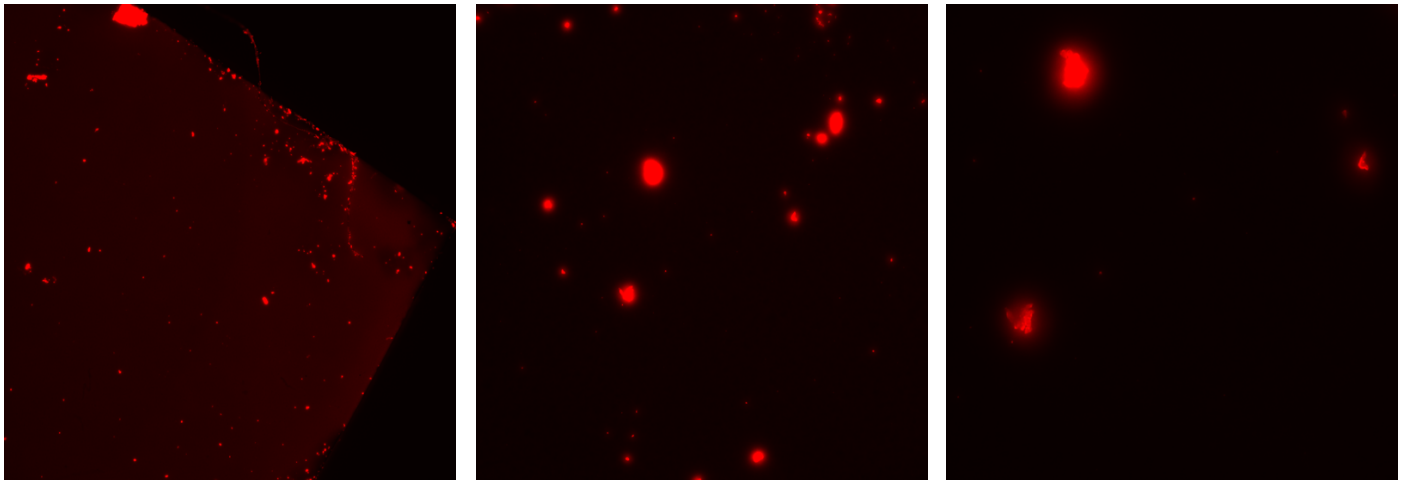

Figure 65: Fluorescence images of porous ZnO thin films after the uptake experiment

Rhodamine has been absorbed on most of the sample surface, while the brighter spots are probably due to the formation of Rhodamine aggregates onto the porous ZnO surface.

From this images, which refers to the sample soaked in the Rhodamine solution for 24h, it is possible to confirm that Rhodamine has been loaded on the ZnO sample, at least on the surface.

From these analyses we cannot know if the Rhodamine was loaded also internally to the porous ZnO structure or just on the surface.

Chapter 5. Conclusions

In this thesis, the bioactivity, biodegradation behaviour and uptake/release properties of porous ZnO thin films deposited by sputtering technique are reported and described.

It is shown that when interacting with SBF, ZnO samples and ZnO samples coated with GO, are bioactive. The interaction of both families of samples with SBF solution induced the precipitation of HAp on the surface. Due to the ability of GO to promote biological interactions, ZnO samples coated with GO showed a better bioactive behaviour, with HAp precipitation manifesting earlier than those without GO coating.

When observing the biodegradation behaviour by soaking the ZnO samples both in SBF and eMEM media, it is found that the crystal structure reminds exactly the same versus the soaking time. On the other hand, it is found that release of Zn^{2+} ions is strongly limited when coating the ZnO surface with GO.

The investigation of porous ZnO thin films for drug delivery applications done using Rhodamine-B as a fluorescent dye successfully showed the ability of this material to uptake and further release molecules. Indeed, porous ZnO thin films were able to uptake molecules after shorts periods of time, and also to release those molecules in a controllable way, to a solution which has ions concentrations nearly equal to those of human blood plasma. Fluorescence microscopy images further confirmed the capacity of porous ZnO thin films to absorb molecules, at least on the surface.

In conclusion, this thesis shows that porous ZnO thin films can be promising candidates for the development of novel ZnO-based biomaterials for tissue engineering and drug delivery applications.

Bibliography

[1] I. D. E., «Principles of Tissue Engineering,» 2000.

[2] Y. L. Y. Z. L. W. J. J. Li Z, «In vitro and in vivo evaluation on the bioactivity of ZnO containing nano-hydroxyapatite/chitosan cement.,» *Biomed Mater Res A. ,* Apr 2010.

[3] Ü. Ö. H. Morkoç, «Zinc Oxide: Fundamentals, Materials and Device Technology,» 2009.

[4] Z. L. Wang, «Mater. Sci. Eng.».

[5] P. M. S. S. A. S. A. V. A. L. G. C. Rossana Gazia, «Photodetection and piezoelectric response from hard and flexible sponge-like ZnO-based structures».

[6] M. Laurenti, «Synthesis and characterization of piezoelectric thin films as functional materials for sensing. PhD thesis,» 2015.

[7] [En línea]. Available: https://ec.europa.eu/health/scientific_committees/opinions_layman/zinc-oxide/es/index.htm#1.

[8] R. D. Braun, «Encyclopedia Britannica,» [En línea]. Available: https://www.britannica.com/science/chemical-analysis/Classical-methods#ref621210.

[9] C. B. J. F. ,. A. F. A. Fortuny, «Bimetallic catalysts for continuous catalytic wet air oxidation of phenol».

[10] J. R. M. S. R. M. S. Rana, «Antimicrobial function of Nd3+-doped anatase titania-coated nickel ferrite composite nanoparticles: A biomaterial system».

[11] W. W. Q. Y. e. a. Liu D, «Surface functionalization of ZnO nanotetrapods with photoactive and electroactive organic monolayers,» Langmuir, 2008.

[12] G. E. W. D. e. a. Taratula O, «Binding studies of molecular linkers to ZnO and MgZnO nanotip films,» J Phys Chem B, 2006.

[13] X. N. W. Z. Zhou J, «Dissolving Behavior and Stability of ZnO Wires in Biofluids: A Study on Biodegradability and Biocompatibility of ZnO Nanostructures,» Adv Mater. , 2006.

[14] L. J. P. A. e. a. Hanley C, «Preferential killing of cancer cells and activated human T cells using ZnO nanoparticles.,» Nanotechnology, 2008.

[15] W. D. E. M. e. a. Wang H, «Fluorescent dye encapsulated ZnO particles with cell-specific toxicity for potential use in biomedical applications.,» J Mater Sci Mater Med., 2009.

[16] K. J. M. M. e. a. Muller KH, «pH-dependent toxicity of high aspect ratio ZnO nanowires in macrophages due to intracellular dissolution.,» ACS Nano., 2010.

[17] P. S. X. T. e. a. George S, «Use of a rapid cytotoxicity screening approach to engineer a safer zinc oxide nanoparticle through iron doping.,» ACS Nano., 2010.

[18] S. A. D. R. V. e. a. Nair S, «Role of size scale of ZnO nanoparticles and microparticles on toxicity toward bacteria and osteoblast cancer cells.,» J Mater Sci Mater Med., 2009.

[19] Z. L. Wang, «Nanostructures of zinc oxide,» *materialstoday,* pp. 26-33, June 2004.

[20] AZoNano, «Zinc Oxide (ZnO) Nanoparticles – Properties, Applications,» 2013.

[21] «ZnO Nanoparticles Growth Properties and Applications,» American Scientific Publishers, 2010.

[22] X. Li, W. Cai, J. An, S. Kim, J. Nah, D. Yang, R. Piner, A. Velamakanni, I. Jung, E. Tutuc, S. K. Banerjee, L. Colombo y R. Ruoff, «R. Science,» 2009.

[23] C. Mattevi, H. Kima y M. Chhowalla, «J. Mater. Chem.,» 2011.

[24] O. C. Compton y S. T. Nguyen, «Small,» 2010.

[25] S. Mao, H. Pu y J. Chen, «RSC Adv.,» 2012.

[26] D. R. Dreyer, S. Park, C. W. Bielawski y R. S. Ruoff, «Chem. Soc. Rev.,» 2010.

[27] S. Gilje, W. Han, M. Wang, K. L. Wang y R. B. Kaner, «Nano Lett.,» 2007.

[28] R. J. S. X. e. a. Liu Z, «PEGylated nanographene oxide for delivery of water-insoluble cancer drugs.,» *J Am Chem Soc,* pp. 10876-10877, 2008.

[29] J. HJ, «Chemical preparation of graphene-based nanomaterials and their applications in chemical and biological sensors,» *Small,* pp. 2413-2427, 2011.

[30] D. S. Guo SJ, «Graphene nanosheet: synthesis, molecular engineering, thin film, hybrids, and energy and analytical applications.,» *Chem Soc Rev.,* pp. 2644-2672, 2011.

[31] A. R. Villalón, «GRAFENO: SÍNTESIS, PROPIEDADES Y APLICACIONES BIOMÉDICAS,» 2016.

[32] H. M. H. T. I. K. M. T. T. A. T. S. R. S. a. M. K. Erika Nishida, «Graphene oxide coating facilitates the bioactivity of scaffold material for tissue engineering,» *Japanese Journal of Applied Physics ,* 13 May 2014.

[33] G.-C. J. Vallet-Regí M, «Calcium phosphates as substitution of bone tissues.,» 2004.

[34] C. Martínez-Pérez, A. Martínez-Villafañe y J. Romero-García, «Formación de hidroxiapatita sobre una superficie polimérica por un método biomimético».

[35] D. C. G. COY, «Obtención y caracterización de hidroxiapatita dopada con nanopartículas de ZnO con potenciales aplicaciones biomédicas».

[36] W. S. Hummers y R. E. Offeman, «"Preparation of Graphitic Oxide",» *Journal of the American Chemical Society,* 20 March 1958.

[37] H. K. S. S. T. K. a. T. Y. T. Kokubo, «"Solutions able to reproduce in vivo surface-structure changes in bioactive glass-ceramic A-W",» *J. Biomed. Mater. Res.,* nº 24, pp. 721-734, 1990.

[38] T. a. H. T. Kokubo, «"How useful is SBF in predicting in vivo bone bioactivity?.",» *Biomaterials,* pp. 2907-2915, 2006.

[39] [En línea]. Available: https://crustal.usgs.gov/laboratories/icpms/intro.html.

[40] [En línea]. Available: https://www.rp-photonics.com/fluorescence_microscopy.html.

[41] I. R. a. W. BONFIELD, «Characterization of hydroxyapatite and carbonated apatite by photo acoustic FTIR spectroscopy,» *JOURNAL OF MATERIALS SCIENCE: MATERIALS IN MEDICINE,* 1997.

[42] A. Kajbafvala, M. Shayegh, M. Mazloumi y S. Sadrnezhaad, «Nanostructure sword-like ZnO wires: Rapid synthesis and characterization through a microwave-assisted route,» Journal of Alloys and Compounds, 2009.

List of Figures

List of Tables